Environmental Science & Technology

pubs.acs.org/est

Article

Mechanisms of Polyethylene Terephthalate Pellet Fragmentation into Nanoplastics and Assimilable Carbons by Wastewater *Comamonas*

Rebecca A. Wilkes, Nanqing Zhou, Austin L. Carroll, Ojaswi Aryal, Kelly P. Teitel, Rebecca S. Wilson, Lichun Zhang, Arushi Kapoor, Edgar Castaneda, Adam M. Guss, Jacob R. Waldbauer, and Ludmilla Aristilde*

Cite This: https://doi.org/10.1021/acs.est.4c06645

Read Online

ACCESS | Metrics & More | Article Recommendations | Supporting Information

ABSTRACT: *Comamonadaceae* bacteria are enriched on poly(ethylene terephthalate) (PET) microplastics in wastewaters and urban rivers, but the PET-degrading mechanisms remain unclear. Here, we investigated these mechanisms with *Comamonas testosteroni*KF-1, a wastewater isolate, by combining microscopy, spectroscopy, proteomics, protein modeling, and genetic engineering. Compared to minor dents on PET films, scanning electron microscopy revealed significant fragmentation of PET pellets, resulting in a 3.5-fold increase in the abundance of small nanoparticles (<100 nm) during 30-day cultivation. Infrared spectroscopy captured primarily hydrolytic cleavage in the fragmented pellet particles. Solution analysis further demonstrated double hydrolysis of a PET oligomer, bis(2-hydroxyethyl) terephthalate, to the bioavailable monomer terephthalate. Supplementation with acetate, a common wastewater co-substrate, promoted cell growth and PET fragmentation. Of the multiple hydrolases encoded in the genome, intracellular proteomics detected only one, which was found in both acetate-only and PET-only conditions. Homology modeling of this hydrolase structure illustrated substrate binding analogous to reported PET hydrolases, despite dissimilar sequences. Mutants lacking this hydrolase gene were incapable of PET oligomer hydrolysis and had a 21% decrease in PET fragmentation; re-insertion of the gene restored both functions. Thus, we have identified constitutive production of a key PET-degrading hydrolase in wastewater *Comamonas*, which could be exploited for plastic bioconversion.

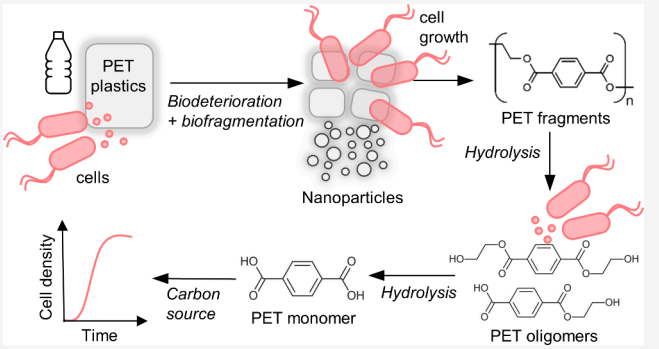

KEYWORDS: *plastic wastes, wastewater, biodegradation, microscopy, proteomics, PET hydrolase*

1. INTRODUCTION

Ubiquitous and extensive usage of plastic materials has led to the accumulation of plastic wastes, which are projected to reach ~33 billion tons by the year 2050.[1] Plastic wastes have been reported in various environments including marine water[2,3] and freshwater,[4,5] sediments,[6,7] and soils.[8,9] Microplastics (MPs) and nanoplastics (NPs), defined operationally as plastic fragments with sizes smaller than 5 mm and 1 μm, respectively, are considered to be a threat to both aquatic and terrestrial ecosystems, as organisms can easily ingest these small particles.[9−11] Since plastic wastes are entirely anthropogenic, wastewater treatment plants (WWTP) represent important repositories for plastics,[12−17] contributing to their release into natural systems and serving as a source of MPs and NPs.[18,19] Wastewater effluents contain various types of MPs, among which polyethylene terephthalate (PET) MPs are the most abundant, constituting approximately 50% of MPs in the effluents.[12] In fact, as an extensively used polymer in disposable plastic containers, PET accounts for 12% of global solid waste.[20] Thus, there is increased research interest focusing on the fate of PET, especially within the context of the biodeterioration and biodegradation of PET plastic materials by WWTP-associated microorganisms.

It is well documented that microorganisms can generate enzymes to deteriorate and modify the surface of PET plastics, facilitating the release of PET MPs and carbon derivatives to be used as carbon sources to support microbial growth.[21,22] Most previous research has focused on microbial consortia[23−27] or a few fungal and bacterial isolates with PET

Received: July 1, 2024
Revised: September 12, 2024
Accepted: September 13, 2024

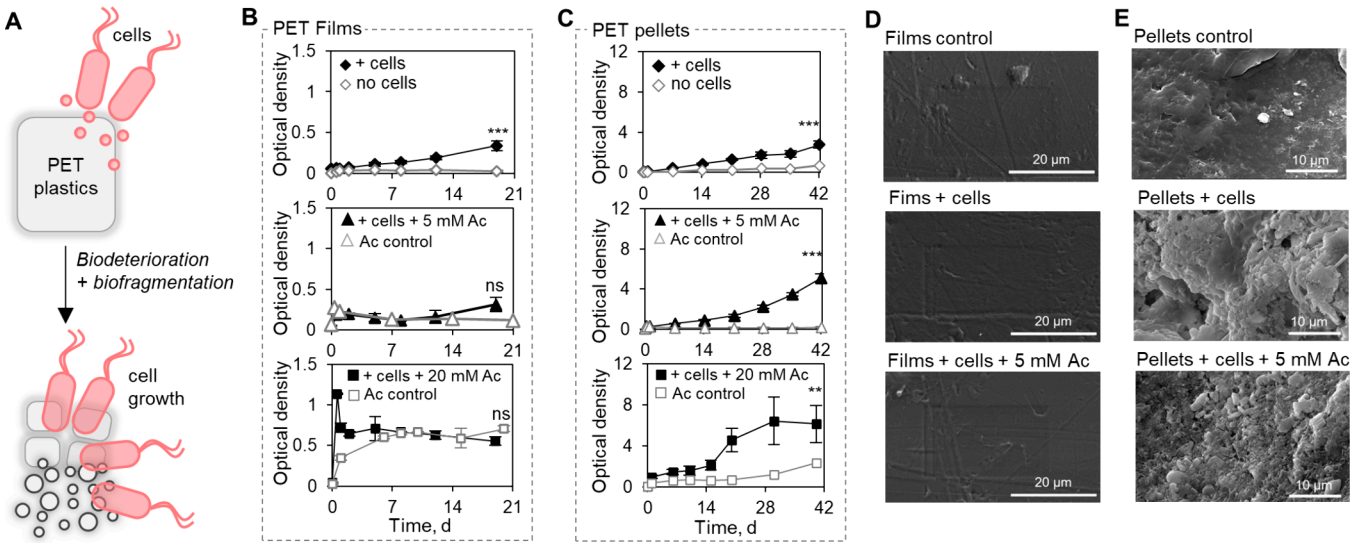

Figure 1. Extent of biofragmentation of PET films and pellets by*C. testosteroni* KF-1. (A) Schematic overview of the investigated steps in PET plastics biodeterioration, biofragmentation, and bioassimilation (B) Cell growth and MP release with (top) PET films as the sole carbon source, (middle) with 5 mM acetate as a co-substrate, or (bottom) with 20 mM acetate as a co-substrate. Control represents cells grown on the two respective acetate concentrations without the PET film. (C) Cell growth and MP release with (top) PET pellets as the sole carbon source, (middle) with 5 mM acetate as a cosubstrate, or (bottom) with 20 mM acetate as a cosubstrate. Control represents cells grown on the two respective acetate concentrations without the PET pellet. (D) Shown are SEM images of washed PET films from the following incubation conditions: with the growth medium with no cells (top), with cells in the growth medium (middle), and with cells in the growth medium supplemented with 5 mM acetate (bottom). (E) Shown are SEM images of washed PET pellets from the following incubation conditions: with the growth medium with no cells (top), with cells in the growth medium (middle), and with cells in the growth medium supplemented with 5 mM acetate (bottom). For (B) and (C), error bars represent the standard deviation of the mean of three biological replicates, and two-tailed *t*-test was performed on the last data points: $*P < 0.05$, $**P < 0.01$, $***P < 0.001$, ns: not significant (ns).

hydrolases, also termed PETases (e.g., IsPETase, FsC, and LCC).[28−34] Of particular interest are the mechanisms through which microorganisms enriched in wastewater sludge can achieve biofragmentation of PET plastics to release MPs, NPs, and eventually the monomer compounds of PET.

Bacteria belonging to the family *Comamonadaceae* have been found to be predominant on MPs that are present in WWTP effluents and urban rivers.[35 −37] Furthermore, colonization of seven different MPs, including PET MPs, with WWTP effluent water consistently led to enriched abundance of the family *Comamonadaceae* compared to the relative distribution of these bacteria in the effluent water.[38] Importantly, as one of the most enriched genera in wastewater sludge,[39,40] the genus *Comamonas* of the family *Comamonadaceae* contains several species with the ability to catabolize a wide spectrum of aromatic compounds,[41−44] including a monomer derivative of PET.[45,46] However, it is not yet known whether wastewater *Comamonas* species possess PET-degrading enzymes that facilitate the depolymerization of PET plastics.

Comamonas testosteroni KF-1, which was isolated from a sewage sludge enrichment as a bacterium that can degrade laundry surfactants,[47] was recently shown to metabolize terephthalate (TPA), a monomer of the PET polymer.[46] Wilkes et al.[46] elucidated the assimilation route of TPA in *C. testosteroni* KF-1 through the 4,5-*meta* cleavage pathway to yield oxaloacetate and pyruvate, two intermediates in the central carbon metabolism. In addition, the genome of *C. testosteroni* KF-1 encodes for multiple hydrolases,[47] which could participate potentially in plastic depolymerization, as demonstrated previously in other microorganisms.[48−52] Yet, it has not yet been demonstrated that *C. testosteroni* and related wastewater *Comamonas* species produce enzymes with PET hydrolase activity to facilitate the biofragmentation of PET materials.[53]

Given prior evidence of colonization of PET plastics by bacteria of the Comamonadacae family,[35−37] we hypothesize that the genome-encoded hydrolases in *C. testosteroni* KF-1 are capable of deteriorating and fragmenting PET plastics, generating bioavailable breakdown products to support bacterial growth (Figure 1A). We tested this hypothesis with PET films and PET pellets incubated with *C. testosteroni* KF-1 by investigating PET biodegradation mechanisms with a suite of orthogonal techniques. First, we monitored the bacterial cell growth and formation of MPs by optical density. Second, we visualized the surface deconstruction and particle morphology of the PET films and pellets by scanning electron microscopy (SEM) and transmission electron microscopy (TEM). Third, we tracked the concentration and sizes of the NPs by nanoparticle tracking analysis. Fourth, we examined the mechanisms of plastic surface modification by attenuated total reflectance-Fourier transform infrared (ATR-FTIR) spectroscopy and confirmed this mechanism by monitoring degradation products of PET pellets and a PET-related oligomer using ultra high-performance liquid chromatography (UHPLC). Fifth, we obtained proteomics data to identify specific hydrolase enzymes produced in response to PET exposure, followed by molecular docking simulations to explore enzyme binding mechanisms informed by previous studies with known PETase structures. Sixth, we deleted the gene that encodes the identified hydrolase from the chromosome of *C. testosteroni* Kf-1 followed by reimplementation of the gene and subsequently determined the hydrolytic activity of the constructed mutants toward PET oligomer and polymer. Additionally, we inserted the *Comamonas* gene into *Pseudomonas putida* KT2440, a widely studied bacterial

https://doi.org/10.1021/acs.est.4c06645
Environ. Sci. Technol. XXXX, XXX, XXX−XXX

platform for waste carbon conversion that lacks PET-degrading capability.[94] The findings presented herein shed light on the mechanisms that afford the growth of wastewater *Comamonas* on PET MPs and advance the consideration of *C. testosteroni* KF-1 as a promising biocatalytic platform for plastic conversion in engineered waste carbon recycling.

2. MATERIALS AND METHODS

2.1. Description of PET Pellets and PET Films. The PET pellets (granular), which were purchased from Sigma-Aldrich (St. Louis, Missouri, USA), had a diameter of 2.5 mm. The PET films, which were purchased from Goodfellow Corporation (Pittsburgh, Pennsylvania, USA), had a thickness of 0.25 mm and were cut in pieces of approximately 2.5 × 1 cm that weigh each about 100 mg. Prior to utilization, the PET pellets and PET film pieces were sterilized with 70% ethanol and air-dried under sterile conditions.

2.2. Bacterial Incubations with PET. The *C. testosteroni* strain KF-1 (DSMZ 14576) (GenBank GCA_000168855.1) was obtained from Deutsche Sammlung für Mikroorganismen and Zellkulturen (Braunschweig, Germany). Stocks of *C. testosteroni* KF-1 cells were stored at −80 °C in Lysogeny broth (Miller) nutrient-rich medium and 25% glycerol. Prior to incubating with the PET materials, the bacterial cells from the stocks were first grown in 5 mL of nutrient-rich Lysogeny broth medium in culture tubes for 12 to 13 h until late exponential phase. Subsequently, the cells were harvested and washed once with a minimal-nutrient medium containing 5.0 mM NaH_2PO_4, 20 mM K_2HPO_4, 37 mM NH_4Cl, 17 mM NaCl, 0.81 mM $MgSO_4{\cdot}7H_2O$, and 34 μM $CaCl_2{\cdot}H_2O$ (pH 7.0). In 125 mL baffled flasks containing 25 mL of the minimal medium, the washed cells were resuspended and inoculated to reach a starting optical density of about 0.05 at 600 nm. Trace metal nutrients and iron were added to the minimal media prior to inoculation, as previously reported.[54] The carbon sources in the minimal media were provided as follows in different experiments: only PET films (1 g per 25 mL of media), PET films supplemented with 5 or 20 mM acetate, PET pellets (1 g per 25 mL of media), PET pellets supplemented with 5 or 20 mM acetate, 2.5 mM of a PET-related oligomer [bis(2-hydroxyethyl) terephthalate, BHET], 3 mM of a PET breakdown product [mono-(2-hydroxyethyl)-terephthalate, MHET], and 3.75 mM of the PET-derived monomer (TPA). The addition of acetate (as sodium acetate) was to test the effects of the presence of a co-substrate typical in WWTP sludge on the PET degradation. Both 5 and 20 mM acetate are within the range (3.8 to 20 mM) used in previous studies with synthetic wastewater.[55−58] Since 5 mM acetate can be carbon-limited for bacterial growth, we also used 20 mM acetate to determine whether higher biomass production would benefit PET degradation. All growth experiments were conducted in three biological replicates in an incubator (New Brunswick Scientific) maintained at 30 °C while being shaken at 220 rpm. Cell growth and the release of MPs were monitored by measuring the optical density at 600 nm (OD_{600}) using an Agilent Cary UV−visible spectrophotometer.

2.3. Monitoring Concentration of PET-Related Compounds. To track the concentration of PET breakdown products at selected time points throughout the incubation period, cell suspensions were pelleted at 10,000*g* and 4 °C for 5 min, and the supernatants were collected and filtered through a spin-filter unit (Costar Spin-X, 0.22 μm-pore-size filter) followed by storage at −20 °C prior to further analysis. Concentrations of BHET, MHET, and TPA were determined using UHPLC with an Agilent ZORBAX Eclipse Plus C18 column (4.6 × 100 mm with 5 μm particle size) and an ultraviolet detector at 240 nm. The mobile phase was composed of 0.1% formic acid (eluent A) and acetonitrile (eluent B) at a flow rate of 0.8 mL min^{-1}. The following fraction of eluent B was applied: 0−5 min, 15−50%; 5−5.5 min, 50−55%; 5.5−5.6 min, 55−15%; 5.6−6 min, 15%. The injection volume was 6 μL, and the column temperature was maintained at 25 °C.

2.4. Microscopic Analysis via SEM and TEM. For these analyses, the PET pellets and films were washed times with sterile 70% ethanol and Milli-Q water to remove bacterial cells. The washed and dried PET materials were fixed onto SEM aluminum sample stubs by using double-sided carbon tapes. Then, the samples were coated with gold platinum or osmium tetroxide and imaged using a Hitachi S-3400N SEM system with an acceleration voltage at 5.0 kV at the Northwestern University Atomic and Nanoscale Characterization Experimental Center (NUANCE).

For TEM imaging, 10 μL of culture suspension was dropped onto glow discharged 200 mesh copper grids with carbon film coating, followed by negative staining with UranyLess EM Stain solution purchased from Electron Microscopy Sciences (Hatfield, Pennsylvania, USA). Then, the grids were washed three times with water and air-dried before imaging. TEM imaging was performed on a JEOL 1400Flash system coupled to a Gatan OneView camera with an acceleration voltage at 120 kV at NUANCE.

2.5. Plastic Surface Analysis by X-ray Diffraction and ATR-FTIR Spectroscopy. With the starting PET films and PET pellets, we obtained X-ray diffraction patterns using a Bruker D8 Advance powder X-ray diffractometer, operated over a 10−40° 2θ Cu Kα angular range (λ = 1.5418 Å) with a 0.02° step size at 3 s per step. We performed ATR-FTIR analysis of PET pellets and films before and after incubation on a Bruker Vertex 70 FTIR spectrophotometer (Billerica, Massachusetts, USA) equipped with a mid-infrared light source, room-temperature DLaTGS detector, KBr beamsplitter, and optic windows. Spectra were collected in a range of 4000 to 600 cm^{-1} at a resolution of 2 cm^{-1} and 64 coadded scans using the MIRacle ATR stage (PIKE) with a single-reflection ZnSe crystal and a pressure clamp. The background was subtracted using OPUS software version 7.2 (Bruker Optics Inc.).

2.6. Nanoparticle Tracking Analysis. Samples for nanoparticle tracking analysis were prepared from 1 mL of cell suspension collected from *C. testosteroni* KF-1 grown on PET pellets with 5 mM acetate as a co-substrate at day 1, day 15, and day 30 of incubation. The cell suspension was pelleted and resuspended in 1 mL of filtered 1× phosphate-buffered saline (PBS) to reach a particle concentration between 10^6 and 10^8 particles/mL. Particle analysis of the independent samples (in five technical replicates) was conducted on a temperature-controlled NanoSight NS300 system (Malvern Panalytical, UK) equipped with a 638 nm laser with a 650 nm long-pass filter and a low flow-cell top-plate in the Analytical bioNanoTechnology Equipment Core Facility of the Simpson Querrey Institute for BioNanotechnology at Northwestern University. The limit for the analysis of PET particle size using nanoparticle tracking analysis is 10 nm.

2.7. Proteomics. Intracellular proteomics were performed on *C. testosteroni* KF-1 cells cultured on PET pellets +5 mM

https://doi.org/10.1021/acs.est.4c06645
Environ. Sci. Technol. XXXX, XXX, XXX−XXX

acetate, PET pellets alone, and 5 mM acetate alone. Cultures (15 mL) were collected at the end of incubation (42 days) and centrifuged at 5000*g* for 10 min at 4 °C to spin down the cells. The pellets were stored at −80 °C until extraction. The proteins in cell pellets were extracted by vortexing in a lysing and denaturing buffer containing SDS (1%), Tris (200 mM, pH 8.0), and dithiothreitol (DTT; 10 mM) for 20 min at 95 °C, followed by incubating the samples in 40 mM iodoacetamide to alkylate the cysteine thiols. Extracellular proteomics were performed on *C. testosteroni* KF-1 cells fed with 2.5 mM BHET alone, 20 mM acetate alone, 2.5 mM BHET with 5 mM acetate, and 3.75 mM TPA alone. Cultures (25 mL) were collected at the late exponential phase and centrifuged at 5000*g* for 10 min at 4 °C to pellet cells. Then, the supernatant was filtered through a 0.22 μm poly(ether sulfone) membrane to remove planktonic cells. The filtrates were collected and stored at −80 °C until protein extraction. Filtrates were first concentrated in a centrifugal filter device (Amicon Ultra, 10 kDa cutoff), and then 4× concentrated denaturing and lysis buffer was added (1× final concentration) to denature and solubilize proteins. To purify proteins away from the abundant polymers in the culture media, the extracellular samples were precipitated in glass centrifuge tubes with four volumes of acetone (−20 °C, overnight) and centrifuged (7197*g*, 1 h), and protein pellets were redissolved in 8 M urea/0.2% deoxycholate/1 M ammonium bicarbonate. The redissolved protein samples were then extracted three times with ethyl acetate to further reduce polymer contaminants.

Protein samples were purified and digested using a modified enhanced filter-aided sample preparation protocol[59] using Sartorius Vivacon 500 concentrators (30 kDa cutoff). The purified proteins were then digested with trypsin at 37 °C overnight. Peptides eluted from the concentrator were dried in a vacuum concentrator and isotopically labeled at both C and N termini using the diDO-IPTL method for downstream quantitative analysis.[60] In brief, C termini were labeled with either ^{16}O or ^{18}O, while the N termini were labeled with either un- or dideuterated formaldehyde (CH_2O or CD_2O).[60] An internal standard was prepared from pooled peptide aliquots labeled with $CH_2O/^{18}O$. ^{16}O-labeled peptide samples were mixed 1:1 (v/v) with ^{18}O-labeled internal standard for quantification.

For liquid chromatography−mass spectrometry (LC-MS) analysis, peptides were separated through a monolithic capillary C_{18} column (GL Sciences MonoCap Ultra, 100 μm inside diameter ×200 cm length) using a water−acetonitrile and 0.1% formic acid gradient (2 to 50% acetonitrile over 180 min) at a flow rate of 360 nL/min on a Dionex UltiMate 3000 LC system with nanoelectrospray ionization (Proxeon Nanospray Flex). High-resolution mass spectra of MS1 parental ion full scan (120,000 $m/\Delta m$) with fragment ion scans of selected precursors were collected on an Orbitrap Elite mass spectrometer (Thermo Fisher) operating in a data-dependent acquisition (DDA) mode. The analysis of mass spectra was performed using MorpheusFromAnotherPlace (MFAP)[60] with annotated protein sequences of *C. testosteroni* KF-1 obtained from the National Center for Biotechnology Information (NCBI) as a search database (accession no. GCF_000168855.1). The mass tolerances of precursor and product ions on MFAP were set at 20 ppm and 0.6 Da, respectively. Modifications were made to include static cysteine carbamidomethylation and variable methionine oxidation, N-terminal (d4)-dimethylation, and C-terminal $^{18}O_2$. The false discovery rate for peptide spectrum matches was controlled to <0.5% using target-decoy searching. The relative abundance and standard errors of proteins were calculated in R using the Arm postprocessing scripts for diDO-IPTL data[60] (github.com/waldbauerlab). Proteomic mass spectral data are available via proteomeXchange under accession number PXD055638 and the MassIVE repository (massive.ucsd.edu) under accession number MSV000095794.

2.8. Protein Homology Modeling and Molecular Docking Simulation. Using the UniProt Align tool for protein sequence alignment analysis, we compared the percent identity of the CtesDRAFT_PD1902 sequence with the sequences of 81 PET-degrading enzymes acquired from the database PlasticDB (sequences and alignment results are provided in the Supplemental Data Set).[61,62] Subsequently, the Advanced Search function in the Research Collaboratory for Structural Bioinformatics Protein Data Bank (RSCB PDB) was used to find an enzyme with reported X-ray crystallography data with the highest sequence similarity to the esterase-type hydrolase (CtesDRAFT_PD1902) identified to be expressed in *C. testosteroni* KF-1 from proteomics. From this exercise, we identified an alkaline esterase Est8 (PDB: 4YPV), which was found in a metagenomic library of a microbial consortium with the capability of degrading diesel oil.[63] Using the *Basic Local Alignment Search Tool* (*BLAST*), it was determined that CtesDRAFT_PD1902 and Est8 had 48% sequence similarity. For the homology modeling, the sequences of the two esterases were aligned using the "Align Sequence Templates" tool in Discovery Studio software. A structural model was developed using the "Build Homology Models" tool to align the sequence of amino acids in CtesDRAFT_PD1902 with those of Est8. This protocol identified sequence motifs in the resulting model of CtesDRAFT_PD1902 that were either identical, strongly similar, or weakly similar to the template sequences of Est8 [Supporting Information (SI), Figure S1]. As discussed in Section 3, several binding motifs reported to be conserved in esterases with PET hydrolase activity were also found in CtesDRAFT_PD1902. An initial structure of BHET, a PET oligomer, was obtained in Discovery Studio using a canonical SMILES string. To simulate binding of the BHET substrate to the CtesDRAFT_PD1902 binding site, both structures were prepared following methods outlined in Koska et al.,[64] with the addition of two Full Minimization steps executed on the BHET model and the assignment of protonation states using the Calculate Protein Ionization and Residue p*K* tool at neutral pH. We then utilized the Flexible Docking protocol to simulate BHET in the binding site of the model enzyme structure, as outlined previously to consider the flexibility of the active site.[64,65]

2.9. Mutant Construction and Examination on BHET Hydrolysis. AG13996 was constructed by deleting CtestDRAFT_PD1902 in the *C. testosteroni* wild-type strain using homologous recombination, as described previously.[46] The 1000 bp regions upstream and downstream of the CtestDRAFT_PD1902 coding sequence were synthesized flanking a NotI restriction site and cloned into a pK18mobsacB vector by GenScript USA, resulting in pALC1026. Wild-type *C. testosteroni* was transformed with this plasmid, and a single crossover mutant was selected using LB agar plates with 50 mg L^{-1} kanamycin. To counterselect for a second crossover, kanamycin-resistant colonies were streaked on LB agar plates supplemented with 100 g L^{-1} sucrose. Deletion of

https://doi.org/10.1021/acs.est.4c06645
Environ. Sci. Technol. XXXX, XXX, XXX−XXX

CtestDRAFT_PD1902 was confirmed by genomic DNA isolation and whole genome sequencing performed by Plasmidsaurus (https://www.plasmidsaurus.com).

In order to re-introduce CtesDRAFT_PD1902 into AG13996, the CtesDRAFT_PD1902 gene sequence was codon- and RBS- sequence optimized for expression in *Pseudomonas putida* KT2440 using the De Novo DNA Operon Calculator[66−68] (https://salislab.net). The optimized sequence was synthesized and cloned into a vector backbone by GenScript USA, forming pALC1022. CtesDRAFT_PD1902 was placed downstream of a *Ptac* promoter with a *lacO* operator, and the plasmid also contains *kanR* and a Bxb1 *attP* sequence for genome integration. Plasmid pALC1022 was introduced into *C. testosteroni* strain AG13996 (genotype: -CtesDRAFT_PD1902), using serine recombinase−assisted genome engineering (SAGE),[69,70] and the previously described transformation protocol for *C. testosteroni*.[46] AG13996 does not contain a Bxb1 *attB* sequence for SAGE, so the integration of pALC1022 occurred semirandomly at a pseudo *attB* sequence in the genome of AG13996.[71] Genomic DNA isolation and whole genome sequencing of the resulting strain, AG14097, was performed by Plasmidsaurus, and it was determined that the CtesDRAFT_PD1902 gene and P*tac* promoter were inserted 17 bases before the start codon of CtesDRAFT_PD5308, which is annotated as an uncharacterized ABC transporter. Plasmid sequences are provided in the Supplemental Data Set.

Heterologous expression of CtesDRAFT_PD1902 in *Pseudomonas putida* KT2440 was performed by introducing plasmid pALC1022 into *P. putida* strain AG5475 (genotype: *P. putida* KT2440 PP_4740-PP_4741::Ptac:tphII operon from *Comamonas* sp. E6 and PP_4217-PP_4218::Ptac:tpaK from *Rhodococcus jostii* RHA1), which was engineered to catabolize TPA, using serine recombinase−assisted genome engineering (SAGE).[69,70] Strain AG5475 does not contain a Bxb1 attB sequence for SAGE, so the integration of pALC1022 occurred semirandomly at a pseudo attB sequence in the genome of AG5475.[71] Genomic DNA isolation and whole genome sequencing of the resulting strain, AG13412, was performed by Plasmidsaurus (https://www.plasmidsaurus.com), and it was determined that two tandem copies of the CtesDRAFT_PD1902 gene and P*tac* promoter were inserted into the PP_3646 locus, which encodes an uncharacterized putative aldehyde dehydrogenase.

We evaluated the hydrolytic activity of *C. testosteroni* mutants toward the PET oligomer, BHET, and PET pellets. The wild-type and mutant strains of *C. testosteroni* were revived from frozen glycerol stocks overnight in LB medium followed by a first transfer to culture tubes containing 5 mL of nutrient minimal media described in Section 2.2 with 5 mM acetate alone or 2.5 mM BHET and 5 mM acetate as the substrates. After reaching the late exponential phase, cells from the first transfer were harvested, washed, and inoculated into 125 mL baffled flasks in triplicate containing 25 mL of the minimal media with 5 mM acetate and 2.5 mM BHET or 1 g PET pellets as a cosubstrate. The growth experiment was conducted under the same conditions as described in Section 2.2. Throughout the incubation, cell growth was monitored by measuring OD_{600}, and the PET oligomers and monomers were quantified using the UHPLC method described in Section 2.3. The same examination of BHET hydrolysis was also performed on the wild-type and mutant strains of *P. putida*.

2.10. Statistical Analysis. The unpaired two-tailed *t*-test was used to evaluate the significance of differences between the two groups. For differences between the three conditions, we applied one-way analysis of variance (ANOVA) combined with Tukey's honestly significant difference (HSD) post hoc test. The *P*-value threshold for statistical significance was 0.05.

3. RESULTS AND DISCUSSION

3.1. Bacterial Growth and Release of MPs from PET Plastics. To assess the surface characterization of the starting PET plastics, we probed the overall crystallinity by X-ray diffraction (XRD), the morphology by SEM, and surface chemistry by FTIR (SI, Figure S2 and S3). The X-ray diffraction patterns captured amorphous features at 12−30° 2θ for the PET pellets and 20−30° 2θ for the PET films, with the PET film displaying relatively higher amorphicity (SI, Figure S2). Interestingly, while the SEM images captured smooth surfaces of the PET films, the surfaces of the PET pellets were irregular with noticeable indents (SI Figure S3). Despite the different surface morphologies, both the PET films and pellets exhibited similar surface chemistry as determined by the vibrational bands of functional groups captured by ATR-FTIR spectroscopy (SI Figure S3). We hypothesized that the morphological differences would affect cell surface attachment and thus influence the extent of the plastics degradation.[52] We monitored the optical density (OD_{600}) as a function of the exposure time of the *C. testosteroni* cells to the PET films and pellets (Figure 1B,C). We obtained 8-fold to 16-fold higher optical density values ($P < 0.001$) when the PET films or pellets were exposed to the *C. testosteroni* KF-1 cells compared to the control experiment in the absence of cells (Figure 1B,C). Therefore, despite the amorphous characteristics of the PET films from nanoscale and subnanoscale features determined by XRD, the microscale features of structural defects captured by SEM were more predictive of the relatively higher extent biofragmentation of the PET pellets than the PET films.

We also conducted experiments with the PET materials co-incubated with acetate, a common volatile fatty acid widely found in WWTP.[72−75] When acetate was present as a co-substrate with the PET materials, we obtained up to 25-fold higher OD_{600} values than with cells grown on acetate alone ($P < 0.001$), either initially in the case of the PET films or throughout the entire experiments in the case of the PET pellets (Figure 1B,C). Therefore, the presence of an additional carbon source, as would be expected in wastewaters, would lead to enhanced biofragmentation of PET plastics, promoting the release of MPs. Due to some increase of OD_{600} intensity caused by minor deterioration of the PET pellets and films to MPs by the nutrient media in the absence of cells, as illustrated in Figure 1B,C, we attributed the increase in OD_{600} values in the presence of cells to both cell growth and, to a relatively minor extent, the fragmentation and release of MPs. We confirmed growth by accounting for colony-forming units on PET pellets alone and PET pellets with acetate, both of which had quantifiable cell numbers (SI Figure S4). Notably, we obtained the highest cell number in the presence of both PET pellets and acetate, which was higher than the sum of cell numbers observed with PET pellets alone and acetate alone, thus implying that acetate promoted the utilization of PET pellets as a carbon source (SI Figure S4). Moreover, plastic weight loss measurements were consistent with the different magnitudes of the OD_{600} values, whereby up to 25-fold higher

https://doi.org/10.1021/acs.est.4c06645
Environ. Sci. Technol. XXXX, XXX, XXX−XXX

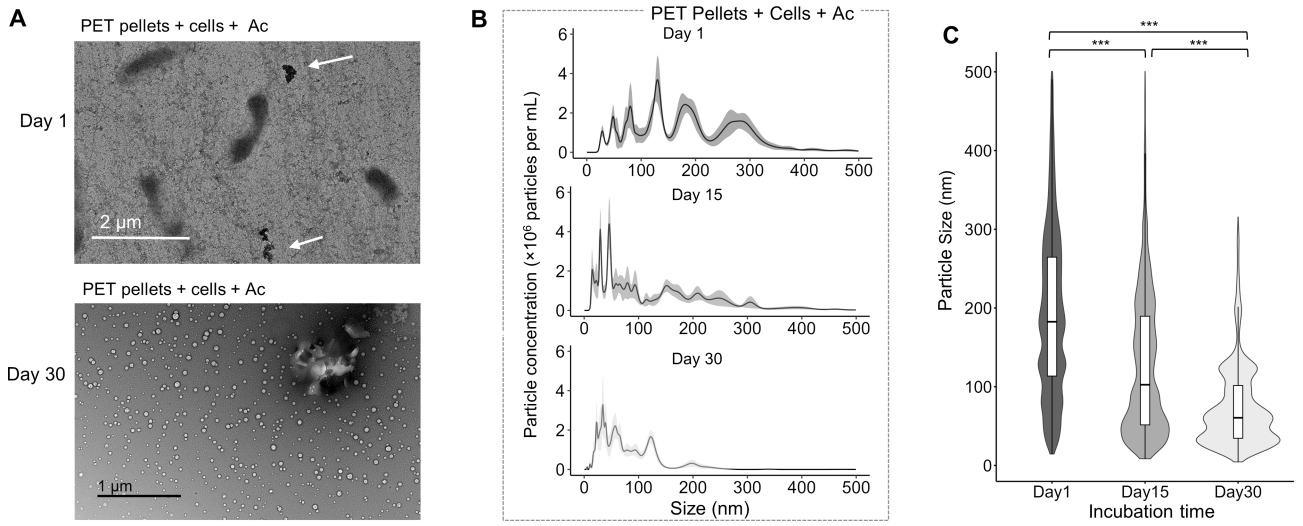

Figure 2. Production of nanoplastic particles from PET pellet fragmentation by*C. testosteroni*. (A) TEM images of suspensions after incubations of *C. testosteroni* with PET pellets and 5 mM acetate (Ac) as a co-substrate for (top) 1 d and (bottom) 30 d. (B) Nanoparticle size concentration and (C) violin plot with inserted box plot of particle size distribution following 1, 15, and 30 days of PET pellets incubated with cells and 5 mM Ac. In (A), white arrows indicate NPs. In (B), the solid lines represent the mean value of the particle concentration, and the shades represent the 95% confidential intervals. In (C), the top and bottom parts of the box plot represent the first and third quartiles, respectively; the line inside represents the median value, and the whiskers represent the upper and lower extremes in the data. The width of the violin plot illustrates the concentration of different particle sizes. In (C), Welch's *t*-test was performed for pairwise comparison due to the unequal sample sizes and variances in different conditions (*$P < 0.05$, **$P < 0.01$, ***$P < 0.001$). Data from an independent duplicate measurement for (B) and (C) are shown in SI, Figure S6.

weight loss with the PET pellets compared to the PET films correlated positively with the up to one order of magnitude higher OD_{600} values when the PET pellets were exposed to the bacterial cells compared to when the PET films were with the cells (SI Figure S5). Next, using SEM and TEM, we probed changes in the polymer surface morphology that would be a consequence of the observed degradation of the PET plastics.

3.2. PET Plastic Surface Modification due to Biodeterioration and Biofragmentation. The deterioration and fragmentation of PET plastics following microbial colonization are expected to alter the morphology of the plastic surface.[26,76] To visualize this morphological alteration at the end of incubation, washed (and dried) PET pellets and PET films were subjected to SEM and FTIR analyses. The surface of the PET films only exhibited very minor changes characterized by some indents on the film surface when acetate was present as a co-substrate; in the absence of acetate in the medium, there were minimal to no alterations of PET film surface, with or without the bacterial cells (Figure 1D). In contrast, the incubation of the PET pellets with the bacterial cells led to an irregular rough surface of the PET pellets with several etched areas; the addition of acetate as an exogenous carbon source enhanced these morphological changes accompanied by deep etches and pitting throughout the surface of the PET pellets (Figure 1E). The PET pellets exposed to the nutrient medium without bacterial cells, however, maintained a relatively smooth-like surface, confirming that the bacterial cells were responsible for the observed changes in the surface morphology of the PET pellets (Figure 1E). Thus, the extent of surface modification illustrated by the SEM images of the PET films and PET pellets was consistent with the different extent of biofragmentation implied by the OD_{600} and plastic weight loss measurements (Figure 1B,C and SI Figure S5).

Due to the elevated OD_{600} values indicating MP release and the SEM images illustrating extensive biodeterioration of the surface of the PET pellets in the presence of *C. testosteroni* KF-1 cells and acetate (Figure 1D,E), we probed for the possible production of both large NPs (100−500 nm) and small NPs (less than 100 nm) from the PET pellets (Figure 2). The TEM images illustrated the evolution of large-sized to small-sized nanoparticles from 1 to 30 days after incubation of the PET pellets (Figure 2A). For quantitative corroboration of the TEM images, we conducted nanoparticle tracking analysis to quantify the distribution of the particles (Figure 2B,C and SI Figure S6). The data revealed that the majority of nanoparticles (79%) were larger than 100 nm after 1 day of incubation, but the particle size was subsequently decreased as a function of incubation time with the bacterial cells (Figure 2B). Specifically, the proportion of the particles smaller than 100 nm increased from 21% on day 1 to 49% on day 15 and to 74% on day 30 (Figure 2C and SI Figure S6). To explore the mechanisms underlying the PET biofragmentation, we performed spectroscopic analysis via ATR-FTIR to reveal the surface chemistry of the PET pellets and subsequently analyzed the products generated from a PET oligomer via UHPLC.

3.3. Production of Assimilable Carbon Products via Hydrolytic Biofragmentation. Both oxidative and hydrolytic reactions are proposed to mediate enzymatic degradation of plastics.[77,78] We investigated which reaction mechanism may be responsible for the PET biofragmentation by *C. testosteroni* KF-1 by monitoring changes in specific functional groups on the surface of the PET films and pellets (Figure 3A,B). We monitored the following functional groups by ATR-FTIR spectroscopy: a broad O−H stretching band at 3263 cm^{-1} in the hydroxyl group,[79] aliphatic C−H stretching vibration bands at 2918 and 2851 cm^{-1},[80] a stretching band of carbonyl group at 1710 cm^{-1},[81] and two C−O stretching bands in the ester group at 1245 and 1097 cm^{-1}[82] (SI Figure S7). To compare the change in these characteristic vibrational bands across the different conditions, we normalized the data by the intensity of the CH_2 bending band at 1410 cm^{-1}, as previously

https://doi.org/10.1021/acs.est.4c06645
Environ. Sci. Technol. XXXX, XXX, XXX−XXX

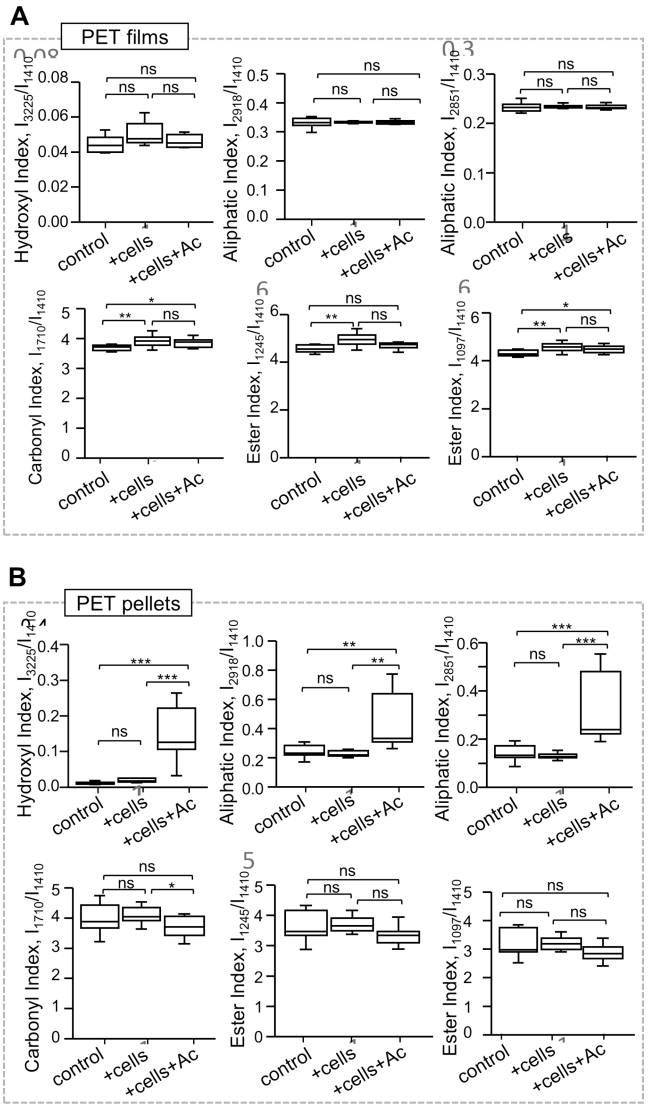

Figure 3. Modifications of the surface chemistry of PET films and pellets after biofragmentation by*C. testosteroni*. Changes in normalized FTIR intensity for different functional groups in (A) PET films (N = 5) after 27-d incubation and (B) PET pellets (N = 6) after 42-d incubation in the following conditions: with the nutrient medium with no cells (control), with cells in the nutrient medium (+cells), with cells in the nutrient medium supplemented with 5 mM acetate (+cells +Ac). In (A) and (B), one-way ANOVA analysis with post hoc Tukey's test was performed: *P < 0.05, **P < 0.01, ***P < 0.001, ns: not significant.

described.[83,84] With the PET films, we observed a small increase (5%, P < 0.01) in the intensity of carbonyl and ester groups, but no significant change in the intensity of hydroxyl or aliphatic groups (Figure 3A). The FTIR data with the PET films thus highlighted minor occurrences of oxidative changes on the film surface. Conversely, with the PET pellets, there was a pronounced increase in the intensities of both hydroxyl group (13-fold increase, P < 0.001) and aliphatic group (69% increase, P < 0.01) compared to the abiotic control (Figure 3B). The significant emergence of the hydroxyl signature on the PET pellets implied that the substantial fragmentation of these pellets was due to hydrolytic cleavage. In sum, the measurable increase in both the carbonyl and hydroxyl indexes implied occurrences of both oxidation and hydrolysis reactions, respectively, with a clear predominance of hydrolysis reactions (Figure 3A,B).

To corroborate further our conclusion from the ATR-FTIR data, we used UHPLC to monitor the hydrolysis of BHET, a PET oligomer analogue, into MHET, a breakdown hydrolytic product of PET, and TPA, a PET monomer from double hydrolysis of BHET (Figure 4A). During a 7-day incubation of the cells with BHET (2.5 mM) as the sole carbon source, we obtained the hydrolytic conversion of 32% of the BHET concentration to MHET, which stayed constant after reaching a plateau (Figure 4B). This latter finding along with growth experiments with the *C. testosteroni* cells led us to conclude that MHET was unlikely to undergo subsequent hydrolysis to TPA or to support cell growth (SI Figure S8). However, direct BHET hydrolysis to TPA via cleavage of the two ester bonds, which has been reported previously with *Candida antarctica*,[85] could not be confirmed here with *C. testosteroni* due to the absence of measurable TPA; we attributed this lack of TPA in solution to rapid assimilation of this bioavailable carbon source by the cells[46] (Figure 4B). In fact, we obtained a near 2-fold or 4.5-fold increase in biomass on BHET alone (P < 0.001) or BHET supplemented with acetate (P < 0.001), respectively; the cell growth was 37% less on acetate alone than on both BHET and acetate (P < 0.001), thus indicating that the hydrolysis of BHET produced bioavailable carbons (Figure 4C). Moreover, in a separate experiment with TPA as a sole carbon source, the bacterial cells fully depleted TPA and grew rapidly on this PET monomer with a doubling time of 19.3 ± 0.1 min^{-1} (Figure 4D); by contrast, we found that ethylene glycol, the other product of BHET hydrolysis, was not able to support the growth of *C. testosteroni* KF-1 as a sole carbon source (SI Figure S8). Therefore, we concluded that the *C. testosteroni* KF-1 cells performed double hydrolysis of BHET to generate bioavailable TPA, which was immediately consumed by the cells to support biomass growth (Figure 4E).

3.4. Enzymes Involved in the Biofragmentation of PET Plastics. To identify the potential hydrolase(s) generated by *C. testosteroni*, KF-1 that would be responsible for PET hydrolysis, both extracellular and intracellular proteomics data were obtained in the presence or absence of PET, with or without acetate (SI Figure S9). Only the intracellular proteomics data sets were used for comprehensive analysis across the different conditions due to the low coverage of the extracellular proteomics data sets, which represented only 10% of the intracellular ones (P < 0.001) (SI Figure S9). Compared to growth on PET alone, we obtained up to 4-fold more (P < 0.05) identified protein spectral counts with cells grown on both PET and acetate or on acetate alone (Figure 5A). Most proteins identified (>95%) in cells grown on PET alone were also present in the acetate-only condition (Figure 5B), but we observed some notable relative abundances of select proteins.

First, comparing when PET was the sole substrate to the acetate-only condition, there was 2.2-fold to 4-fold lower abundance of enzymes (citrate synthase, aconitate hydratase, and succinate dehydrogenase) involved in the tricarboxylic acid (TCA) cycle in the central carbon metabolism (P < 0.01) (Figure 5C). In contrast to the routing of PET-derived aromatic carbons first through a cleavage pathway prior to entry into the TCA cycle, there would be direct influx of acetate-derived carbons into the TCA cycle, thus explaining the need for relatively higher abundance of enzymes in the TCA cycle for the acetate-only condition, especially when regulation for initial aromatic carbon catabolism has been

https://doi.org/10.1021/acs.est.4c06645
Environ. Sci. Technol. XXXX, XXX, XXX−XXX

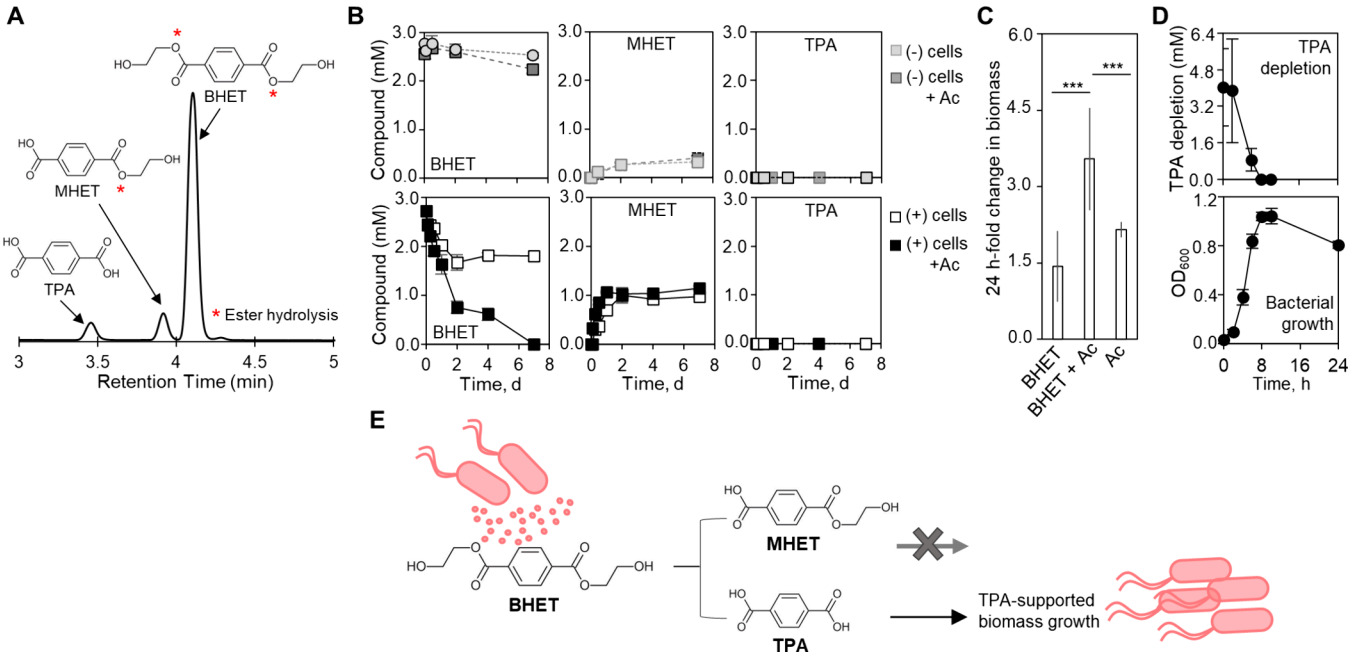

Figure 4. Production of bioavailable monomer from hydrolysis of PET oligomer by *C. testosteroni*. (A) UHPLC spectrum of the quantification of BHET, a PET-related oligomer, and its ester hydrolysis products, MHET and TPA. (B) Tracking the depletion of 2.5 mM BHET and corresponding production of MHET and TPA in (top) the absence and (bottom) the presence of *C. testosteroni* KF-1 cells. (C) Fold change in biomass growth from starting cell abundance after 24 h of growth on 2.5 mM BHET alone, a mixture of 2.5 mM BHET and 5 mM acetate (Ac), or 5 mM Ac. (D) (Top) Depletion of TPA and (bottom) associated biomass growth with *C. testosteroni* KF-1 grown on 3.75 mM TPA as the only carbon source. (E) Schematic illustration of biotransformation of PET-related oligomer to an assimilable PET monomer by *C. testosteroni* KF-1. In (C), two-tailed *t*-test was performed: $*P < 0.05$, $**P < 0.01$, $***P < 0.001$.

reported to be via transcriptional regulation of the cleavage pathway.[46] Second, we also identified 2.1-fold to 4.2-fold higher abundance of a flagellin protein (FliC, $P < 0.05$), a copper-resistant protein (CopC, $P < 0.001$), and an organic hydroperoxide resistance protein (CtesDRAFT_PD0278, $P < 0.01$) in the presence of PET (Figure 5C), all of which would facilitate higher cell mobility and stress tolerance during the biodeterioration activity observed on the solid plastic surface. The enzymes that were uniquely found in cells incubated with PET alone or with acetate were associated primarily with ribosomal protein, transcriptional regulators, and flagellin synthesis (SI Table S1, S2).

Of the 39 hydrolases annotated in the *C. testosteroni* KF-1 genome, the only one identified in our intracellular proteomics data was CtesDRAFT_PD1902, an esterase/lipase-type hydrolase that was present in the cells grown on PET alone, PET with acetate, and acetate alone (Figure 5C). There was no significant difference in the abundance of the identified esterase-type hydrolase cells grown on PET alone versus those grown on acetate alone ($P = 0.35$), or PET with acetate versus acetate alone ($P = 0.25$), implying that *C. testosteroni* constitutively produced this enzyme, irrespective of its exposure to PET specifically.

Analysis of the percent identity of the CtesDRAFT_PD1902 sequence with 81 known sequences of PET-degrading enzymes[61,62] revealed that it was not a homologue (<20% identity) of any known cutinase/lipase, PETase, BHETase, or MHETase reported in other microbes (Supplemental Data Set). Based on sequence similarity, a homology model structure of CtesDRAFT_PD1902 was constructed with Est8, a structurally characterized esterase cloned from a microbial consortium that exhibited diesel oil-degrading capability[63] (Figure 5D). Interestingly, in the model structure of our identified esterase-type hydrolase in *C. testosteroni*, there were several binding motifs previously found to be conserved in esterases with reported PET hydrolase activity:[65,86−90] the residues in the catalytic triad (Ser158, Asp253, and His283), the 85HGGG88 motif that constitutes the oxyanion hole, and two esterase catalytic motifs (^{156}GXSXG^{160} and ^{253}DPXXD^{257}) (Figure 5D).

Importantly, optimized binding of BHET in the predicted binding site of the structural model of the enzyme revealed key distances between BHET atoms and catalytic residues in the enzyme that were consistent with previous reports from PETase enzymes (Figure 5E).[63,90] Specifically, the distance between EO2 of Asp253 and EN2 of His283 was 2.888 Å (compared to 2.633 Å[63]), the distance between EN1 of His283 and EO1 of Ser158 was 3.244 Å (compared to 2.664 Å[63]), and the distance between EO1 of Ser158 and the carbonyl carbon BC7 of BHET was 4.770 Å (Figure 5E). The latter distance was within 4% of the analogous distance between the catalytic serine and the carbonyl carbon of nP-hexanoate (4.6 Å) in a crystal structure of another alkaline esterase (E53; PDB: 6KEU),[90] which has been compared previously with Est8 and PETase.[63,91] This distance was reported to be catalytically important due to the requirement of the serine residue to perform a nucleophilic attack on the carbonyl carbon of the ester moiety in the bound substrate. Our modeling investigations thus revealed that the esterase-type hydrolase CtesDRAFT_PD1902 produced in both the presence and absence of PET by *C. testosteroni* exhibited the required binding conformation to catalyze the hydrolysis of BHET, a PET oligomer. Therefore, we hypothesized that *C. testosteroni*

https://doi.org/10.1021/acs.est.4c06645
Environ. Sci. Technol. XXXX, XXX, XXX−XXX

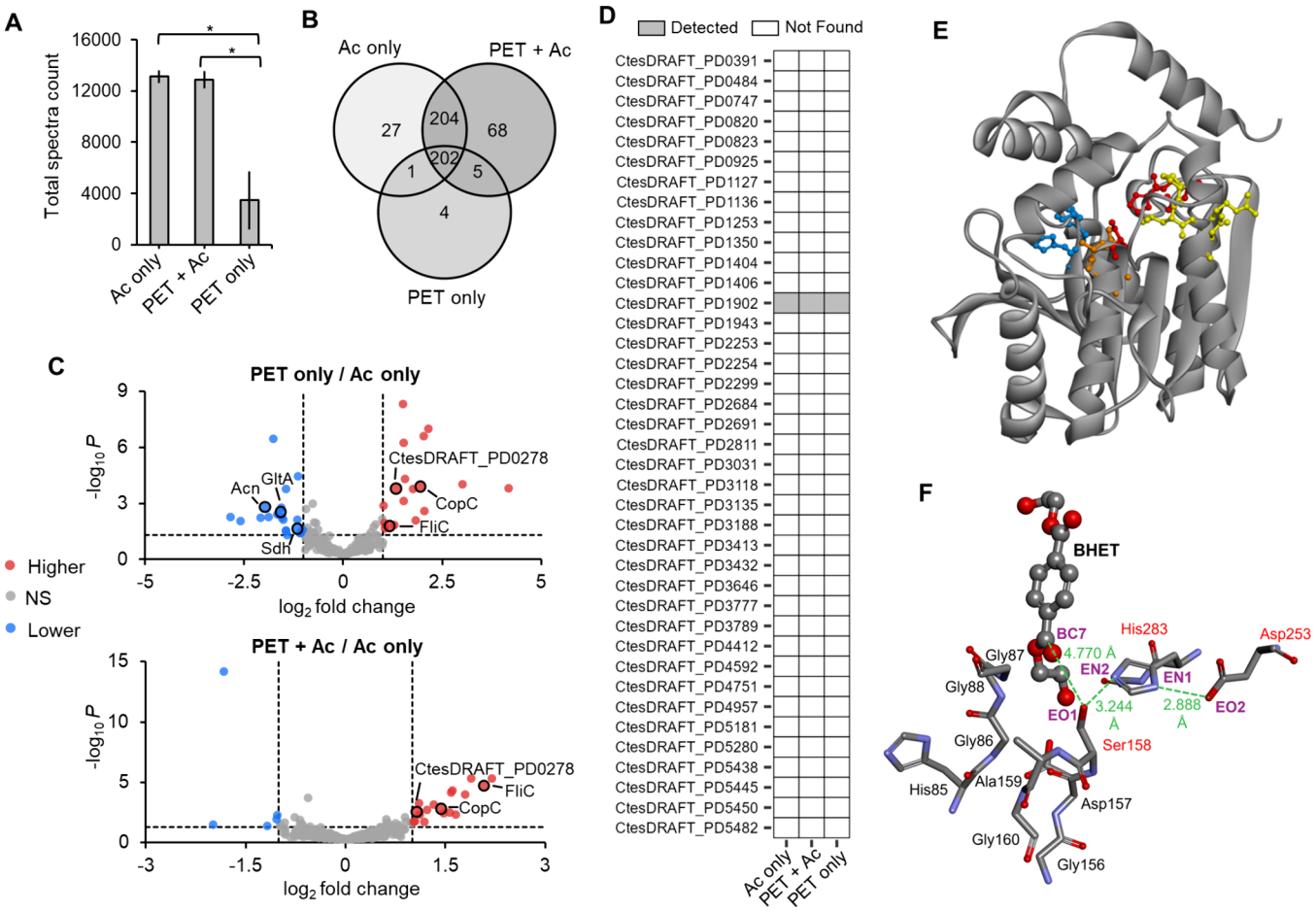

Figure 5. Proteomics analysis and protein homology modeling of candidate hydrolases in*C. testosteroni*. (A) Total spectral count identified from intracellular proteomics of *C. testosteroni* KF-1 grown on acetate (Ac) alone, both PET and Ac, and PET alone. (B) Venn diagrams of the proteins identified from the intracellular proteomics data with each condition. (C) Volcano plots of adjusted *P* value for significance (*y* axis) versus $\log_2$ fold change (*x* axis) in the abundance of proteins in (top) cells fed on PET relative to cells fed on Ac alone or (bottom) cells fed on both PET and acetate relative to cells on acetate alone. (D) Proteomics profiling of hydrolases encoded in the genome of *C. testosteroni* KF-1. (E) Homology modeling of the identified hydrolase (CtesDRAFT_PD1902) and shown in color are several binding site motifs conserved in esterase-type hydrolases with reported PET activity: catalytic residues (Ser158, Asp253, and His283; red); the 85HGGG88 motif (blue), two esterase catalytic motifs, 156GXSXG160 in orange, and 253DPXXD257 in yellow. (F) Optimized binding of BHET in the predicted binding site of the modeled hydrolase structure. In (A), (B), and (D), data were obtained from four biological replicates. In (A), two-tailed *t* test was performed: $*P < 0.05$, $**P < 0.01$, $***P < 0.001$. In (C), significant difference in protein abundances ($|\log_2$ fold change$| > 1$ and $P < 0.05$) are indicated in red (higher abundance) and blue (lower abundance); gray dots represent genes without significant changes (NS) in protein levels. In (C), selected proteins are labeled: aconitate hydratase (Acn); citrate synthase (GltA); succinate dehydrogenase (Sdh); flagellin protein (FliC); copper resistance protein (CopC); a gene encoding an organic hydroperoxide resistance protein (CtesDRAFT_PD0278). In (F), amino acid residues are labeled with their three-letter codes and sequence numbers; key atoms are noted in purple. Important distances between BHET and catalytic residues are shown in green.

constitutively produced this PET-degrading enzyme, which does not require the presence of PET to induce its production.

3.5. Confirmation of Hydrolase Function for PET Breakdown by *C. testosteroni*. To test this hypothesis, we investigated the fragmentation activity of the secretions of the acetate-fed *C. testosteroni* KF-1 toward the PET films and pellets (SI Figure S10A). The release of MPs was observed after incubating PET films or pellets with the cell-free secretions (SI Figure S10A), thus indicating that *C. testosteroni* KF-1 secreted enzymes to catalyze the hydrolysis of PET polymer despite the absence of PET in the growth medium. Furthermore, we incubated cell-free secretions from acetate-grown cells at pH 7 with BHET (2.1 mM) and obtained a 56% depletion in the BHET concentration accompanied by the production and accumulation of both MHET and TPA, the two subsequent breakdown products from single and double hydrolysis reactions of BHET (SI Figure S10B). The accumulation of MHET and TPA accounted for 44 and 13% of the starting BHET molar concentration, respectively, correlating with the 56% loss of BHET (SI Figure S10B). The notable presence of TPA in the cell-free reaction contrasted with the previously discussed immediate consumption of TPA when the *C. testosteroni* cells were present (Figure 4B), which was consistent with the proposed rapid assimilation of TPA by *C. testosteroni*.

To verify that the identified hydrolase (CtesDRAFT_PD1902) was involved in conferring hydrolytic activity in *C. testosteroni* KF-1, we constructed a mutant strain (AG13996) that lacked this hydrolase gene; we also prepared another strain (AG14097) in which the gene was re-inserted (Figure 6A). Without CtesDRAFT_PD1902, strain AG13996 lost the ability to degrade the PET oligomer, BHET (Figure

https://doi.org/10.1021/acs.est.4c06645
Environ. Sci. Technol. XXXX, XXX, XXX−XXX

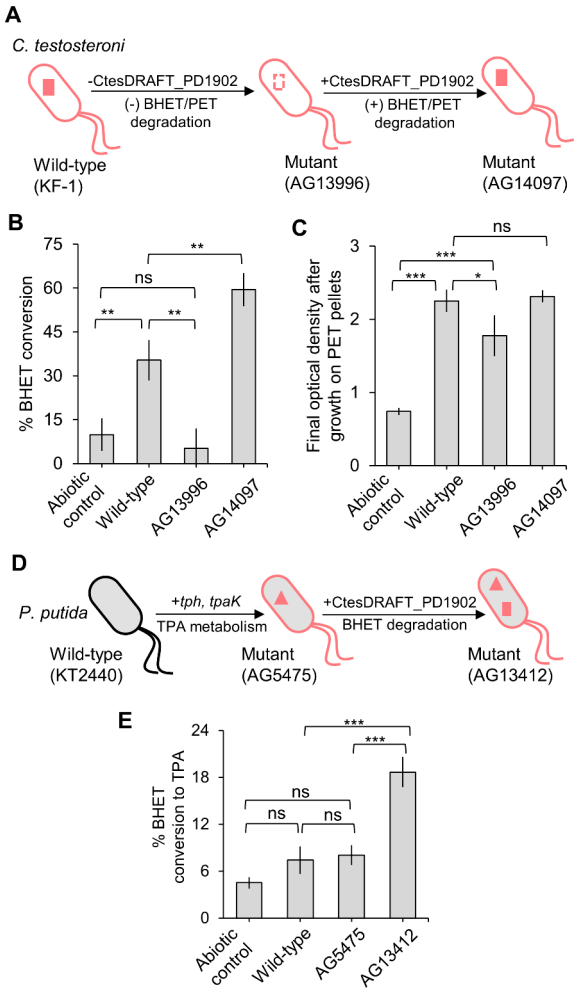

Figure 6. Confirming functions of the identified hydrolase from*C. testosteroni*. (A) Schematic illustration of genetic engineering to delete CtesDRAFT_PD1902 and reintroduce the gene back to *C. testosteroni* after the deletion. (B) Percentage of BHET conversion when incubated with *C. testosteroni* wild-type and mutant strains in the presence of 5 mM acetate as a co-substrate for 48 h. (C) Final optical density (OD_{600}) from PET pellets when incubated with *C. testosteroni* wild-type and mutant strains in the presence of 5 mM acetate as a co-substrate for 19 days. (D) Schematic illustration of heterologous expression of TPA utilization and CtesDRAFT_PD1902 genes in *P. putida* KT2440. (E) Percentage of BHET hydrolysis to TPA when incubated with the different strains in the presence of 5 mM acetate as a co-substrate for 48 h. One-way ANOVA with post hoc Tukey's test was performed. $*P < 0.05$, $**P < 0.01$, $***P < 0.001$, ns: not significant.

6B). Following re-insertion of the hydrolase gene in the deletion mutant, the resulting strain AG14097 recovered the function of BHET degradation, remarkably at 69% higher than the wild-type *C. testosteroni* KF-1 (Figure 6B). Additionally, we tested the possibility that both mutant strains could degrade PET pellets. The final optical density with strain AG13996 was 21% lower compared to the wild-type *C. testosteroni* strain ($P < 0.05$), but still 2.4-fold higher than the abiotic control ($P < 0.001$) (Figure 6C). With strain AG14097 with the re-inserted gene, the final optical density was not significantly different from the wild-type culture (Figure 6C). These data thus indicated that the identified hydrolase contributed to a significant extent to the biofragmentation of PET polymer, but was involved likely in concert with other enzymes because the ability to degrade the PET polymer was not lost completely when the gene was removed (Figure 6C). For instance, in our extracelluar proteomics data obtained with secretions from *C. testosteroni* KF-1 grown on acetate only, we had identified a hydrolase encoded by CtesDRAFT_PD3135, which was previously characterized as a steroid esterase involved in a steroid cleavage pathway.[92] It is possible that this additional hydrolase (CtesDRAFT_PD3135) identified in the *Comomonas* secretions could participate along with CtesDRAFT_PD1902 to enhance PET breakdown, but this remains to be confirmed.

We further tested the function of CtesDRAFT_PD1902 in a biotechnologically relevant microbial host, *Pseudomonas putida* KT2440,[93] which does not possess either TPA utilization or BHET-degrading capabilities. We genetically modified a previously engineered *P. putida* KT2440 strain (AG5475), which contains a TPA utilization pathway adopted from *Comamonas* sp. E6,[94] to express the CtesDRAFT_PD1902 gene identified here from *C. testosteroni* KF-1, resulting in strain AG13412 (Figure 6D). After growing all three *P. putida* strains (KT2440, AG5475, and AG13412) on BHET and acetate as a co-substrate, we did not obtain BHET conversion to TPA by the wild-type strain ($P = 0.16$) nor the AG5475 strain ($P = 0.08$) relative to the abiotic control (Figure 6E). However, endowed with the CtesDRAFT_PD1902 gene, AG13412 was able to achieve nearly 3-fold more BHET conversion to TPA than the wild-type and AG5475 strains (Figure 6E) ($P < 0.001$). Extensive biochemical studies of the identified hydrolases are beyond the scope of our investigation. It would be worthwhile for future studies to evaluate the reactivity kinetics of our PET-degrading enzyme relative to other previously reported PETases and related enzymes. Collectively, our data with the engineered strains demonstrated that the identified hydrolase from the intracellular proteomics was responsible for the observed hydrolysis of PET oligomer by *C. testosteroni* KF-1, and it also contributed in part to the biofragmentation of the PET polymer.

3.6. Implications for the Fate of PET Plastics in WWTPs and Biotechnology. Wastewater treatment plants represent an important repository of MPs materials, including notably PET. Wastewater-residing bacteria with plastic-degrading capabilities play an important role in the fate of these materials. Here, we combined microscopic and spectroscopic techniques with proteomics, structural modeling, and genetic engineering to investigate the mechanisms that facilitate reported enrichment of *Comamonas*-related species on PET MPs in WWTPs and rivers.[35−37] In summary, we demonstrated that *C. testosteroni* constitutively produced a hydrolase that can facilitate fragmentation of PET plastics to generate NPs and breakdown products available for bacterial assimilation. Although *C. testosteroni* KF-1 was initially classified as a human pathogen,[101,102] its low virulence led to it being assigned the same biosafety level as *Escherichia coli* strain K12. This suggests the potential for broader applications of *C. testosteroni* KF-1.

We revealed systematically several steps in the bioconversion of PET by *C. testosteroni* KF-1, including biodeterioration and biofragmentation to promote the generation of enzyme binding sites with the release of MPs and NPs, the hydrolysis of the PET oligomer, and the assimilation of the PET monomer for bacterial biomass growth. Our data thus suggested the possible *in situ* production of PET NPs in WWTPs by wastewater *Comamonas,* which can potentially be

https://doi.org/10.1021/acs.est.4c06645
Environ. Sci. Technol. XXXX, XXX, XXX−XXX

harmful to biota in receiving waters.[95,96] However, evidence of complete degradation of the PET materials to support bacterial growth implied that *C. testosteroni* cells exhibit attractive traits that can be exploited for the engineered bioconversion of plastics. Based on bioinformatics query of the genome, it was previously concluded that *Comamonas* sp. E6 does not possess homologues of known PETases,[53] similar to our conclusion here with *C. testosteroni* KF-1. Importantly, we identified a hydrolase in *C. testosteroni* KF-1 with confirmed catalytic activity for the hydrolysis of a PET oligomer. Despite dissimilar sequence identity with reported PETases, our homology protein modeling revealed that the model structure of the identified hydrolase possessed the catalytic triad of the conserved binding motifs in esterases with previously reported PET hydrolase activity.[65,86−90] Protein purification and characterization are needed to evaluate the kinetics of this enzyme.

Moreover, despite similar surface chemistry, we found that the rough-like surface of the PET pellets was more amendable to biofragmentation than the smooth-like surface of the PET films, indicating a dependence of biofragmentation on the plastics morphology. The purpose of this study was not to determine in detail how the physical characteristics of PET films versus PET pellets influenced the extent of biodeterioration. To determine this relationship, further investigation is warranted.

As confirmation of the function of the newly identified hydrolase from *C. testosteroni*, we demonstrated impaired and recovered degradation of BHET and PET in knockout and reimplementation strains, respectively. Implementation of this *Comamonas* hydrolase gene in *Pseudomonas putida* KT2440,[93] a biotechnologically relevant bacterium that natively lacks PET-degrading capability, enabled hydrolysis of a PET oligomer. It is worthwhile to note that *C. testosteroni* naturally produces polyhydroxyalkanoate, a polymer widely considered an important precursor to biodegradable plastics.[97−100] Therefore, in addition to the depolymerization and assimilation steps, further conversion of the PET-derived carbons to value-added products could be achieved in *C. testosteroni* as a microbial platform. Despite being initially classified as a human pathogen,[101,102] *Comamonas* species are considered important environmental bacteria widely detected in soils and wastewater sludge.[102] To leverage *C. testosteroni* as a microbial platform for plastic upcycling,[103] future research needs to evaluate and optimize the channeling of the PET-derived compounds to high yields of polyhydroxyalkanoate or other value-added products in this species.

It is well known that *C. testosteroni* and related bacteria have a preference for gluconeogenic organic substrates, which include short-chain organic acids also termed volatile fatty acids such as acetate and succinate.[54,104] The expression of the newly identified hydrolase in *C. testosteroni* KF-1 was observed during growth on either only PET or only acetate, a common volatile fatty acid found in WWTP solutions,[72−75] as the sole carbon source. Therefore, we posit that organic acids widely found in WWTPs can promote the secretion of hydrolases to initiate the biotransformation of PET plastics by wastewater *Comamonas*.

Based on the complex composition of plastic wastes in WWTPs,[12,13] the degradation capability of *C. testosteroni* and related species toward other plastics materials is worthy of consideration. For instance, *C. testosteroni* has been shown to grow on dicarboxylates of various carbon lengths (from six carbons to 10 carbons),[101] all of which are potential breakdown products of polypropylene and polyethylene plastics.[105,106] Whether the multiple hydrolases in *C. testosteroni* and other wastewater *Comamonas* spp. are capable of degrading different plastic polymers has not yet been explored. Given the diversity of microbial communities in WWTPs,[107] future investigations also need to consider the effect of interspecies interactions alongside *Comamonas* on the fate of PET and other plastics in wastewaters. Beyond *Comamonas* species, our study presents a technical roadmap demonstrating the application of a suite of orthogonal techniques to interrogate the underlying mechanisms in the natural bioconversion of plastic waste by environmental microbes.

■ ASSOCIATED CONTENT

Supporting Information

The Supporting Information is available free of charge at https://pubs.acs.org/doi/10.1021/acs.est.4c06645.

Protein sequence of PETases used for alignment, percent identify matrix of the alignment result, extracellular proteomics data, intracellular proteomics data, and the plasmid sequences used for the construction of the mutants (PDF)

■ AUTHOR INFORMATION

Corresponding Author

Ludmilla Aristilde − *Department of Civil and Environmental Engineering, McCormick School of Engineering and Applied Science and Northwestern Center for Synthetic Biology, Northwestern University, Evanston, Illinois 60208, United States;* orcid.org/0000-0002-8566-1486; Phone: 847-491-2999; Email: ludmilla.aristilde@northwestern.edu

Authors

Rebecca A. Wilkes − *Department of Civil and Environmental Engineering, McCormick School of Engineering and Applied Science, Northwestern University, Evanston, Illinois 60208, United States*

Nanqing Zhou − *Department of Civil and Environmental Engineering, McCormick School of Engineering and Applied Science, Northwestern University, Evanston, Illinois 60208, United States*

Austin L. Carroll − *Biosciences Division, Oak Ridge National Laboratory, Oak Ridge, Tennessee 37831, United States*

Ojaswi Aryal − *Department of Civil and Environmental Engineering, McCormick School of Engineering and Applied Science, Northwestern University, Evanston, Illinois 60208, United States*

Kelly P. Teitel − *Department of Civil and Environmental Engineering, McCormick School of Engineering and Applied Science, Northwestern University, Evanston, Illinois 60208, United States;* orcid.org/0000-0001-9001-5369

Rebecca S. Wilson − *Department of Civil and Environmental Engineering, McCormick School of Engineering and Applied Science, Northwestern University, Evanston, Illinois 60208, United States*

Lichun Zhang − *Department of the Geophysical Sciences, University of Chicago, Chicago, Illinois 60637, United States*

Arushi Kapoor − *Department of Civil and Environmental Engineering, McCormick School of Engineering and Applied*

https://doi.org/10.1021/acs.est.4c06645
Environ. Sci. Technol. XXXX, XXX, XXX−XXX

Science, Northwestern University, Evanston, Illinois 60208, United States

Edgar Castaneda − *Northwestern Center for Synthetic Biology, Northwestern University, Evanston, Illinois 60208, United States*

Adam M. Guss − *Biosciences Division, Oak Ridge National Laboratory, Oak Ridge, Tennessee 37831, United States*

Jacob R. Waldbauer − *Department of the Geophysical Sciences, University of Chicago, Chicago, Illinois 60637, United States;* orcid.org/0000-0002-0338-6143

Complete contact information is available at: https://pubs.acs.org/10.1021/acs.est.4c06645

Notes

The authors declare the following competing financial interest(s): L.A., R.A.W., J.R.W., A.C., A.G., and N.Z. are inventors on U.S. provisional patent 63/695,951 relating to biofragmentation of PET by genetically engineered bacterial [#]strains.

[#]R.A.W. and N.Z. are co-first authors.

■ ACKNOWLEDGMENTS

This research was funded by the U.S. National Science Foundation (NSF) (CHE-2109097) awarded to L.A. This work was authored, in part, by Oak Ridge National Laboratory, which is managed by UT-Battelle, LLC, for the US Department of Energy (DOE) under contract DE-AC05-00OR22725. Funding was provided, in part, by the US DOE, Office of Energy Efficiency and Renewable Energy, Advanced Materials and Manufacturing Technologies Office (AMMTO) and Bioenergy Technologies Office as part of the BOTTLE Consortium. We thank Jiaxing Wang of the Aristilde Research Group (Northwestern University) for collecting the XRD spectra of PET films and pellets.

■ REFERENCES

(1) Rochman, C. M.; Browne, M. A.; Halpern, B. S.; Hentschel, B. T.; Hoh, E.; Karapanagioti, H. K.; Rios-Mendoza, L. M.; Takada, H.; Teh, S.; Thompson, R. C. Classify Plastic Waste as Hazardous. *Nature* **2013**, *494* (7436), 169−171.

(2) Law, K. L. Plastics in the Marine Environment. *Annual Review of Marine Science* **2017**, *9* (1), 205−229.

(3) Carney Almroth, B.; Eggert, H. Marine Plastic Pollution: Sources, Impacts, and Policy Issues. *Review of Environmental Economics and Policy* **2019**, *13* (2), 317−326.

(4) van Emmerik, T.; Schwarz, A. Plastic Debris in Rivers. *WIREs Water* **2020**, *7* (1), No. e1398.

(5) Cable, R. N.; Beletsky, D.; Beletsky, R.; Wigginton, K.; Locke, B. W.; Duhaime, M. B. Distribution and Modeled Transport of Plastic Pollution in the Great Lakes, the World's Largest Freshwater Resource. *Front. Environ. Sci.* **2017**, *5*, 45.

(6) Corcoran, P. L.; Norris, T.; Ceccanese, T.; Walzak, M. J.; Helm, P. A.; Marvin, C. H. Hidden Plastics of Lake Ontario, Canada and Their Potential Preservation in the Sediment Record. *Environ. Pollut.* **2015**, *204*, 17−25.

(7) Martin, C.; Baalkhuyur, F.; Valluzzi, L.; Saderne, V.; Cusack, M.; Almahasheer, H.; Krishnakumar, P. K.; Rabaoui, L.; Qurban, M. A.; Arias-Ortiz, A.; Masqué, P.; Duarte, C. M. Exponential Increase of Plastic Burial in Mangrove Sediments as a Major Plastic Sink. *Science Advances* **2020**, *6* (44), No. eaaz5593.

(8) Huo, Y.; Dijkstra, F. A.; Possell, M.; Singh, B. Chapter One - Plastics in Soil Environments: All Things Considered. In *Advances in Agronomy*; Sparks, D. L., Ed.; Academic Press, 2022; Vol. *175*, pp 1−132. .

(9) Qi, Y.; Yang, X.; Pelaez, A. M.; Huerta Lwanga, E.; Beriot, N.; Gertsen, H.; Garbeva, P.; Geissen, V. Macro- and Micro- Plastics in Soil-Plant System: Effects of Plastic Mulch Film Residues on Wheat (Triticum Aestivum) Growth. *Science of The Total Environment* **2018**, *645*, 1048−1056.

(10) Hurley, R. R.; Woodward, J. C.; Rothwell, J. J. Ingestion of Microplastics by Freshwater Tubifex Worms. *Environ. Sci. Technol.* **2017**, *51* (21), 12844−12851.

(11) Courtene-Jones, W.; Clark, N. J.; Fischer, A. C.; Smith, N. S.; Thompson, R. C. Ingestion of Microplastics by Marine Animals. In *Plastics and the Ocean*; ; John Wiley & Sons, Ltd, 2022; pp 349−366. .

(12) Wolff, S.; Kerpen, J.; Prediger, J.; Barkmann, L.; Müller, L. Determination of the Microplastics Emission in the Effluent of a Municipal Waste Water Treatment Plant Using Raman Microspectroscopy. *Water Research X* **2019**, *2*, No. 100014.

(13) Van Do, M.; Le, T. X. T.; Vu, N. D.; Dang, T. T. Distribution and Occurrence of Microplastics in Wastewater Treatment Plants. *Environmental Technology & Innovation* **2022**, *26*, No. 102286.

(14) Conley, K.; Clum, A.; Deepe, J.; Lane, H.; Beckingham, B. Wastewater Treatment Plants as a Source of Microplastics to an Urban Estuary: Removal Efficiencies and Loading per Capita over One Year. *Water Research X* **2019**, *3*, No. 100030.

(15) Kazour, M.; Terki, S.; Rabhi, K.; Jemaa, S.; Khalaf, G.; Amara, R. Sources of Microplastics Pollution in the Marine Environment: Importance of Wastewater Treatment Plant and Coastal Landfill. *Mar. Pollut. Bull.* **2019**, *146*, 608−618.

(16) Okoffo, E. D.; O'Brien, S.; O'Brien, J. W.; Tscharke, B. J.; Thomas, K. V. Wastewater Treatment Plants as a Source of Plastics in the Environment: A Review of Occurrence, Methods for Identification, Quantification and Fate. *Environmental Science: Water Research & Technology* **2019**, *5* (11), 1908−1931.

(17) Zhang, J.; Wang, L.; Halden, R. U.; Kannan, K. Polyethylene Terephthalate and Polycarbonate Microplastics in Sewage Sludge Collected from the United States. *Environ. Sci. Technol. Lett.* **2019**, *6* (11), 650−655.

(18) Sol, D.; Laca, A.; Laca, A.; Díaz, M. Approaching the Environmental Problem of Microplastics: Importance of WWTP Treatments. *Science of The Total Environment* **2020**, *740*, No. 140016.

(19) Frehland, S.; Kaegi, R.; Hufenus, R.; Mitrano, D. M. Long-Term Assessment of Nanoplastic Particle and Microplastic Fiber Flux through a Pilot Wastewater Treatment Plant Using Metal-Doped Plastics. *Water Res.* **2020**, *182*, No. 115860.

(20) Benyathiar, P.; Kumar, P.; Carpenter, G.; Brace, J.; Mishra, D. K. Polyethylene Terephthalate (PET) Bottle-to-Bottle Recycling for the Beverage Industry: A Review. *Polymers* **2022**, *14* (12), 2366.

(21) Sheth, M. U.; Kwartler, S. K.; Schmaltz, E. R.; Hoskinson, S. M.; Martz, E. J.; Dunphy-Daly, M. M.; Schultz, T. F.; Read, A. J.; Eward, W. C.; Somarelli, J. A. Bioengineering a Future Free of Marine Plastic Waste. *Frontiers in Marine Science* **2019**, *6*, 624.

(22) Maity, S.; Banerjee, S.; Biswas, C.; Guchhait, R.; Chatterjee, A.; Pramanick, K. Functional Interplay between Plastic Polymers and Microbes: A Comprehensive Review. *Biodegradation* **2021**, *32* (5), 487−510.

(23) Qi, X.; Ma, Y.; Chang, H.; Li, B.; Ding, M.; Yuan, Y. Evaluation of PET Degradation Using Artificial Microbial Consortia. *Frontiers in Microbiology* **2021**, *12*, No. 778828.

(24) Meyer-Cifuentes, I. E.; Werner, J.; Jehmlich, N.; Will, S. E.; Neumann-Schaal, M.; Öztürk, B. Synergistic Biodegradation of Aromatic-Aliphatic Copolyester Plastic by a Marine Microbial Consortium. *Nat. Commun.* **2020**, *11* (1), 5790.

(25) Cao, Z.; Yan, W.; Ding, M.; Yuan, Y. Construction of Microbial Consortia for Microbial Degradation of Complex Compounds. *Frontiers in Bioengineering and Biotechnology* **2022**, *10*, 1051233.

(26) Maheswaran, B.; Al-Ansari, M.; Al-Humaid, L.; Sebastin Raj, J.; Kim, W.; Karmegam, N.; Mohamed Rafi, K. In Vivo Degradation of Polyethylene Terephthalate Using Microbial Isolates from Plastic Polluted Environment. *Chemosphere* **2023**, *310*, No. 136757.

(27) Roberts, C.; Edwards, S.; Vague, M.; León-Zayas, R.; Scheffer, H.; Chan, G.; Swartz, N. A.; Mellies, J. L. Environmental Consortium

Containing Pseudomonas and Bacillus Species Synergistically Degrades Polyethylene Terephthalate Plastic. *mSphere* **2020**, *5* (6), e01151−20.
(28) Dang, T. C. H.; Nguyen, D. T.; Thai, H.; Nguyen, T. C.; Tran, T. T. H.; Le, V. H.; Nguyen, V. H.; Tran, X. B.; Pham, T. P. T.; Nguyen, T. G.; Nguyen, Q. T. Plastic Degradation by Thermophilic Bacillus Sp. BCBT21 Isolated from Composting Agricultural Residual in Vietnam. *Adv. Nat. Sci: Nanosci. Nanotechnol.* **2018**, *9* (1), No. 015014.
(29) Tanasupawat, S.; Takehana, T.; Yoshida, S.; Hiraga, K.; Oda, K. Ideonella Sakaiensis Sp. Nov., Isolated from a Microbial Consortium That Degrades Poly(Ethylene Terephthalate). *International Journal of Systematic and Evolutionary Microbiology* **2016**, *66* (8), 2813−2818.
(30) Weigert, S.; Perez-Garcia, P.; Gisdon, F. J.; Gagsteiger, A.; Schweinshaut, K.; Ullmann, G. M.; Chow, J.; Streit, W. R.; Höcker, B. Investigation of the Halophilic PET Hydrolase PET6 from Vibrio Gazogenes. *Protein Sci.* **2022**, *31* (12), No. e4500.
(31) Sarkhel, R.; Sengupta, S.; Das, P.; Bhowal, A. Comparative Biodegradation Study of Polymer from Plastic Bottle Waste Using Novel Isolated Bacteria and Fungi from Marine Source. *J. Polym. Res.* **2020**, *27* (1), 16.
(32) Taniguchi, I.; Yoshida, S.; Hiraga, K.; Miyamoto, K.; Kimura, Y.; Oda, K. Biodegradation of PET: Current Status and Application Aspects. *ACS Catal.* **2019**, *9* (5), 4089−4105.
(33) Xu, A.; Zhou, J.; Blank, L. M.; Jiang, M. Future Focuses of Enzymatic Plastic Degradation. *Trends in Microbiology* **2023**, *31* (7), 668−671.
(34) Khairul Anuar, N. F. S.; Huyop, F.; Ur-Rehman, G.; Abdullah, F.; Normi, Y. M.; Sabullah, M. K.; Abdul Wahab, R. An Overview into Polyethylene Terephthalate (PET) Hydrolases and Efforts in Tailoring Enzymes for Improved Plastic Degradation. *Int. J. Mol. Sci.* **2022**, *23* (20), 12644.
(35) McCormick, A.; Hoellein, T. J.; Mason, S. A.; Schluep, J.; Kelly, J. J. Microplastic Is an Abundant and Distinct Microbial Habitat in an Urban River. *Environ. Sci. Technol.* **2014**, *48* (20), 11863−11871.
(36) McCormick, A. R.; Hoellein, T. J.; London, M. G.; Hittie, J.; Scott, J. W.; Kelly, J. J. Microplastic in Surface Waters of Urban Rivers: Concentration, Sources, and Associated Bacterial Assemblages. *Ecosphere* **2016**, *7* (11), No. e01556.
(37) Martínez-Campos, S.; Redondo-Nieto, M.; Shang, J.; Peña, N.; Leganés, F.; Rosal, R.; Fernandez-Piñas, F. Characterization of Microbial Colonization and Diversity in Reverse Osmosis Membrane Autopsy. *dwt* **2018**, *131*, 9−29.
(38) Martínez-Campos, S.; González-Pleiter, M.; Fernández-Piñas, F.; Rosal, R.; Leganés, F. Early and Differential Bacterial Colonization on Microplastics Deployed into the Effluents of Wastewater Treatment Plants. *Science of The Total Environment* **2021**, *757*, No. 143832.
(39) Huang, Y.; Hou, X.; Liu, S.; Ni, J. Correspondence Analysis of Bio-Refractory Compounds Degradation and Microbiological Community Distribution in Anaerobic Filter for Coking Wastewater Treatment. *Chemical Engineering Journal* **2016**, *304*, 864−872.
(40) Zhan, J.; Han, Y.; Xu, S.; Wang, X.; Guo, X. Succession and Change of Potential Pathogens in the Co-Composting of Rural Sewage Sludge and Food Waste. *Waste Management* **2022**, *149*, 248−258.
(41) Locher, H. H.; Leisinger, T.; Cook, A. M. Degradation of P-Toluenesulphonic Acid via Sidechain Oxidation, Desulphonation and Meta Ring Cleavage in Pseudomonas (Comamonas) testosteroni T-2. *Microbiology* **1989**, *135* (7), 1969−1978.
(42) Okai, M.; Ohki, Y.; Yamamoto, S.; Takashio, M.; Ishida, M.; Urano, N. Comamonas Sp. 3ah48 Is a Dibenz[a,h]Anthracene-degrading Bacterium That Is Tolerant to Heavy Metals. *Letters in Applied Microbiology* **2019**, *68* (6), 589−596.
(43) Dutton, J. R.; Venables, W. A.; Saint, C. P. Comamonas Acidovorans UCC61 Catabolizes O-Phthalate via a 4,5-Oxygenation Pathway That Is Encoded on a 70 Kbp Section of Plasmid pOPH1 Bounded by Directly Repeated Sequences. *Microbiology* **1995**, *141* (7), 1673−1682.
(44) Providenti, M. A.; O'Brien, J. M.; Ruff, J.; Cook, A. M.; Lambert, I. B. Metabolism of Isovanillate, Vanillate, and Veratrate by Comamonas testosteroni Strain BR6020. *J. Bacteriol.* **2006**, *188* (11), 3862−3869.
(45) Kincannon, W. M.; Zahn, M.; Clare, R.; Lusty Beech, J.; Romberg, A.; Larson, J.; Bothner, B.; Beckham, G. T.; McGeehan, J. E.; DuBois, J. L. Biochemical and Structural Characterization of an Aromatic Ring-Hydroxylating Dioxygenase for Terephthalic Acid Catabolism. *Proc. Natl. Acad. Sci. U. S. A.* **2022**, *119* (13), No. e2121426119.
(46) Wilkes, R. A.; Waldbauer, J.; Caroll, A.; Nieto-Domínguez, M.; Parker, D. J.; Zhang, L.; Guss, A. M.; Aristilde, L. Complex Regulation in a Comamonas Platform for Diverse Aromatic Carbon Metabolism. *Nat. Chem. Biol.* **2023**, 651−662.
(47) Weiss, M.; Kesberg, A. I.; LaButti, K. M.; Pitluck, S.; Bruce, D.; Hauser, L.; Copeland, A.; Woyke, T.; Lowry, S.; Lucas, S.; Land, M.; Goodwin, L.; Kjelleberg, S.; Cook, A. M.; Buhmann, M.; Thomas, T.; Schleheck, D. Permanent Draft Genome Sequence of Comamonas testosteroni KF-1. *Stand in Genomic Sci.* **2013**, *8* (2), 239−254.
(48) von Haugwitz, G.; Han, X.; Pfaff, L.; Li, Q.; Wei, H.; Gao, J.; Methling, K.; Ao, Y.; Brack, Y.; Mican, J.; Feiler, C. G.; Weiss, M. S.; Bednar, D.; Palm, G. J.; Lalk, M.; Lammers, M.; Damborsky, J.; Weber, G.; Liu, W.; Bornscheuer, U. T.; Wei, R. Structural Insights into (Tere)Phthalate-Ester Hydrolysis by a Carboxylesterase and Its Role in Promoting PET Depolymerization. *ACS Catal.* **2022**, *12* (24), 15259−15270.
(49) Son, H. F.; Cho, I. J.; Joo, S.; Seo, H.; Sagong, H.-Y.; Choi, S. Y.; Lee, S. Y.; Kim, K.-J. Rational Protein Engineering of Thermo-Stable PETase from Ideonella Sakaiensis for Highly Efficient PET Degradation. *ACS Catal.* **2019**, *9* (4), 3519−3526.
(50) Ribitsch, D.; Yebra, A. O.; Zitzenbacher, S.; Wu, J.; Nowitsch, S.; Steinkellner, G.; Greimel, K.; Doliska, A.; Oberdorfer, G.; Gruber, C. C.; Gruber, K.; Schwab, H.; Stana-Kleinschek, K.; Acero, E. H.; Guebitz, G. M. Fusion of Binding Domains to Thermobifida Cellulosilytica Cutinase to Tune Sorption Characteristics and Enhancing PET Hydrolysis. *Biomacromolecules* **2013**, *14* (6), 1769−1776.
(51) Herzog, K.; Müller, R.-J.; Deckwer, W.-D. Mechanism and Kinetics of the Enzymatic Hydrolysis of Polyester Nanoparticles by Lipases. *Polym. Degrad. Stab.* **2006**, *91* (10), 2486−2498.
(52) Wilkes, R. a.; Aristilde, L. Degradation and Metabolism of Synthetic Plastics and Associated Products by Pseudomonas Sp.: Capabilities and Challenges. *J. Appl. Microbiol.* **2017**, *123* (3), 582−593.
(53) Knott, B. C.; Erickson, E.; Allen, M. D.; Gado, J. E.; Graham, R.; Kearns, F. L.; Pardo, I.; Topuzlu, E.; Anderson, J. J.; Austin, H. P.; Dominick, G.; Johnson, C. W.; Rorrer, N. A.; Szostkiewicz, C. J.; Copié, V.; Payne, C. M.; Woodcock, H. L.; Donohoe, B. S.; Beckham, G. T.; McGeehan, J. E. Characterization and Engineering of a Two-Enzyme System for Plastics Depolymerization. *Proc. Natl. Acad. Sci. U.S.A.* **2020**, *117* (41), 25476−25485.
(54) Wilkes, R. A.; Waldbauer, J.; Aristilde, L. Analogous Metabolic Decoupling in Pseudomonas Putida and Comamonas testosteroni Implies Energetic Bypass to Facilitate Gluconeogenic Growth. *mBio* **2021**, *12* (6), e03259−21.
(55) Ha, J. H.; Ong, S. K. Nitrification and Denitrification in Partially Aerated Biological Aerated Filter (BAF) with Dual Size Sand Media. *Water Sci. Technol.* **2007**, *55* (1−2), 9−17.
(56) Mitra, S.; Gupta, S. K. Pilot-Scale Treatment of a Trichloethylene Rich Synthetic Wastewater in Anaerobic Hybrid Reactor, with Morphological Study of the Sludge Granules. *Clean Techn Environ. Policy* **2014**, *16* (5), 947−956.
(57) Kumar, R.; Venugopalan, V. P. Development of Self-Sustaining Phototrophic Granular Biomass for Bioremediation Applications. *Curr. Sci.* **2015**, *108* (9), 1653−1661.
(58) Prakash, S. M.; Gupta, S. K. Biodegradation of Tetrachloroethylene in Upflow Anaerobic Sludge Blanket Reactor. *Bioresour. Technol.* **2000**, *72* (1), 47−54.

https://doi.org/10.1021/acs.est.4c06645
Environ. Sci. Technol. XXXX, XXX, XXX−XXX

(59) Erde, J.; Loo, R. R. O.; Loo, J. A. Enhanced FASP (eFASP) to Increase Proteome Coverage and Sample Recovery for Quantitative Proteomic Experiments. *J. Proteome Res.* **2014**, *13* (4), 1885−1895.
(60) Waldbauer, J.; Zhang, L.; Rizzo, A.; Muratore, D. diDO-IPTL: A Peptide-Labeling Strategy for Precision Quantitative Proteomics. *Anal. Chem.* **2017**, *89* (21), 11498−11504.
(61) Gambarini, V.; Pantos, O.; Kingsbury, J. M.; Weaver, L.; Handley, K. M.; Lear, G. *Phylogenetic Distribution of Plastic-Degrading Microorganisms. mSystems* **2021**, *6*, 1.
(62) Gambarini, V.; Pantos, O.; Kingsbury, J. M.; Weaver, L.; Handley, K. M.; Lear, G. PlasticDB: A Database of Microorganisms and Proteins Linked to Plastic Biodegradation. *Database (Oxford)* **2022**, *2022*, baac008.
(63) Pereira, M. R.; Maester, T. C.; Mercaldi, G. F.; de Macedo Lemos, E. G.; Hyvönen, M.; Balan, A. From a Metagenomic Source to a High-Resolution Structure of a Novel Alkaline Esterase. *Appl. Microbiol. Biotechnol.* **2017**, *101* (12), 4935−4949.
(64) Koska, J.; Spassov, V. Z.; Maynard, A. J.; Yan, L.; Austin, N.; Flook, P. K.; Venkatachalam, C. M. Fully Automated Molecular Mechanics Based Induced Fit Protein−Ligand Docking Method. *J. Chem. Inf. Model.* **2008**, *48* (10), 1965−1973.
(65) Fecker, T.; Galaz-Davison, P.; Engelberger, F.; Narui, Y.; Sotomayor, M.; Parra, L. P.; Ramírez-Sarmiento, C. A. Active Site Flexibility as a Hallmark for Efficient PET Degradation by *I. Sakaiensis* PETase. *Biophys. J.* **2018**, *114* (6), 1302−1312.
(66) Cetnar, D. P.; Salis, H. M. Systematic Quantification of Sequence and Structural Determinants Controlling mRNA Stability in Bacterial Operons. *ACS Synth. Biol.* **2021**, *10* (2), 318−332.
(67) Reis, A. C.; Salis, H. M. An Automated Model Test System for Systematic Development and Improvement of Gene Expression Models. *ACS Synth. Biol.* **2020**, *9* (11), 3145−3156.
(68) Halper, S. M.; Hossain, A.; Salis, H. M. Synthesis Success Calculator: Predicting the Rapid Synthesis of DNA Fragments with Machine Learning. *ACS Synth. Biol.* **2020**, *9* (7), 1563−1571.
(69) Elmore, J. R.; Furches, A.; Wolff, G. N.; Gorday, K.; Guss, A. M. Development of a High Efficiency Integration System and Promoter Library for Rapid Modification of *Pseudomonas Putida* KT2440. *Metabolic Engineering Communications* **2017**, *5*, 1−8.
(70) Elmore, J. R.; Dexter, G. N.; Baldino, H.; Huenemann, J. D.; Francis, R.; Peabody, G. L.; Martinez-Baird, J.; Riley, L. A.; Simmons, T.; Coleman-Derr, D.; Guss, A. M.; Egbert, R. G. High-Throughput Genetic Engineering of Nonmodel and Undomesticated Bacteria via Iterative Site-Specific Genome Integration. *Science Advances* **2023**, *9* (10), No. eade1285.
(71) Combes, P.; Till, R.; Bee, S.; Smith, M. C. M. The Streptomyces Genome Contains Multiple Pseudo-attB Sites for the (Phi)C31-Encoded Site-Specific Recombination System. *J. Bacteriol.* **2002**, *184* (20), 5746−5752.
(72) Ucisik, A. S.; Henze, M. Biological Hydrolysis and Acidification of Sludge under Anaerobic Conditions: The Effect of Sludge Type and Origin on the Production and Composition of Volatile Fatty Acids. *Water Res.* **2008**, *42* (14), 3729−3738.
(73) Reyhanitash, E.; Kersten, S. R. A.; Schuur, B. Recovery of Volatile Fatty Acids from Fermented Wastewater by Adsorption. *ACS Sustainable Chem. Eng.* **2017**, *5* (10), 9176−9184.
(74) Agnihotri, S.; Yin, D.-M.; Mahboubi, A.; Sapmaz, T.; Varjani, S.; Qiao, W.; Koseoglu-Imer, D. Y.; Taherzadeh, M. J. A Glimpse of the World of Volatile Fatty Acids Production and Application: A Review. *Bioengineered 13* (1), 1249−1275. .
(75) Longo, S.; Katsou, E.; Malamis, S.; Frison, N.; Renzi, D.; Fatone, F. Recovery of Volatile Fatty Acids from Fermentation of Sewage Sludge in Municipal Wastewater Treatment Plants. *Bioresour. Technol.* **2015**, *175*, 436−444.
(76) Gong, J.; Kong, T.; Li, Y.; Li, Q.; Li, Z.; Zhang, J. Biodegradation of Microplastic Derived from Poly(Ethylene Terephthalate) with Bacterial Whole-Cell Biocatalysts. *Polymers (Basel)* **2018**, *10* (12), 1326.
(77) Mohanan, N.; Montazer, Z.; Sharma, P. K.; Levin, D. B. Microbial and Enzymatic Degradation of Synthetic Plastics. *Frontiers in Microbiology* **2020**, *11*, No. 580709.
(78) Cai, Z.; Li, M.; Zhu, Z.; Wang, X.; Huang, Y.; Li, T.; Gong, H.; Yan, M. Biological Degradation of Plastics and Microplastics: A Recent Perspective on Associated Mechanisms and Influencing Factors. *Microorganisms* **2023**, *11* (7), 1661.
(79) Parry, S. A.; Pawley, A. R.; Jones, R. L.; Clark, S. M. An Infrared Spectroscopic Study of the OH Stretching Frequencies of Talc and 10-A Phase to 10 GPa. *Am. Mineral.* **2007**, *92* (4), 525−531.
(80) Cervantes-Uc, J. M.; Espinosa, J. I. M.; Cauich-Rodríguez, J. V.; Ávila-Ortega, A.; Vázquez-Torres, H.; Marcos-Fernández, A.; San Román, J. TGA/FTIR Studies of Segmented Aliphatic Polyurethanes and Their Nanocomposites Prepared with Commercial Montmorillonites. *Polym. Degrad. Stab.* **2009**, *94* (10), 1666−1677.
(81) Almond, J.; Sugumaar, P.; Wenzel, M. N.; Hill, G.; Wallis, C. Determination of the Carbonyl Index of Polyethylene and Polypropylene Using Specified Area under Band Methodology with ATR-FTIR Spectroscopy. *e-Polym.* **2020**, *20* (1), 369−381.
(82) Van Der Weerd, J.; Van Loon, A.; Boon, J. J. FTIR Studies of the Effects of Pigments on the Aging of Oil. *Studies in Conservation* **2005**, *50* (1), 3−22.
(83) Drobota, M.; Persin, Z.; Zemljic, L.; Mohan, T.; Stana-Kleinschek, K.; Doliska, A.; Bracic, M.; Ribitsch, V.; Harabagiu, V.; Coseri, S. Chemical Modification and Characterization of Poly-(Ethylene Terephthalate) Surfaces for Collagen Immobilization. *Open Chemistry* **2013**, *11* (11), 1786−1798.
(84) Donelli, I.; Freddi, G.; Nierstrasz, V. A.; Taddei, P. Surface Structure and Properties of Poly-(Ethylene Terephthalate) Hydrolyzed by Alkali and Cutinase. *Polym. Degrad. Stab.* **2010**, *95* (9), 1542−1550.
(85) Świderek, K.; Velasco-Lozano, S.; Galmés, M. À.; Olazabal, I.; Sardon, H.; López-Gallego, F.; Moliner, V. Mechanistic Studies of a Lipase Unveil Effect of pH on Hydrolysis Products of Small PET Modules. *Nat. Commun.* **2023**, *14*, 3556.
(86) Austin, H. P.; Allen, M. D.; Donohoe, B. S.; Rorrer, N. A.; Kearns, F. L.; Silveira, R. L.; Pollard, B. C.; Dominick, G.; Duman, R.; El Omari, K.; Mykhaylyk, V.; Wagner, A.; Michener, W. E.; Amore, A.; Skaf, M. S.; Crowley, M. F.; Thorne, A. W.; Johnson, C. W.; Woodcock, H. L.; McGeehan, J. E.; Beckham, G. T. Characterization and Engineering of a Plastic-Degrading Aromatic Polyesterase. *Proc. Natl. Acad. Sci. U. S. A.* **2018**, *115* (19), E4350−E4357.
(87) Liu, B.; He, L.; Wang, L.; Li, T.; Li, C.; Liu, H.; Luo, Y.; Bao, R. Protein Crystallography and Site-Direct Mutagenesis Analysis of the Poly(Ethylene Terephthalate) Hydrolase PETase from Ideonella Sakaiensis. *ChemBioChem.* **2018**, *19* (14), 1471−1475.
(88) Joo, S.; Cho, I. J.; Seo, H.; Son, H. F.; Sagong, H.-Y.; Shin, T. J.; Choi, S. Y.; Lee, S. Y.; Kim, K.-J. Structural Insight into Molecular Mechanism of Poly(Ethylene Terephthalate) Degradation. *Nat. Commun.* **2018**, *9* (1), 382.
(89) Han, X.; Liu, W.; Huang, J.-W.; Ma, J.; Zheng, Y.; Ko, T.-P.; Xu, L.; Cheng, Y.-S.; Chen, C.-C.; Guo, R.-T. Structural Insight into Catalytic Mechanism of PET Hydrolase. *Nat. Commun.* **2017**, *8* (1), 2106.
(90) Ding, Y.; Nie, L.; Yang, X.-C.; Li, Y.; Huo, Y.-Y.; Li, Z.; Gao, Y.; Cui, H.-L.; Li, J.; Xu, X.-W. Mechanism and Structural Insights Into a Novel Esterase, E53, Isolated From Erythrobacter Longus. *Frontiers in Microbiology* **2022**, *12*, No. 798194.
(91) Jerves, C.; Neves, R. P. P.; Ramos, M. J.; da Silva, S.; Fernandes, P. A. Reaction Mechanism of the PET Degrading Enzyme PETase Studied with DFT/MM Molecular Dynamics Simulations. *ACS Catal.* **2021**, *11* (18), 11626−11638.
(92) Weiß, M. *Bacterial Degradation Pathways for Xenobiotic and Natural Organosulfonates*. Ph.D. Dissertation, an der Universität Konstanz, 2014.
(93) de Lorenzo, V.; Pérez-Pantoja, D.; Nikel, P. I. Pseudomonas Putida KT2440: The Long Journey of a Soil-Dweller to Become a Synthetic Biology Chassis. *J. Bacteriol.* **2024**, *0* (0), e00136−24.

https://doi.org/10.1021/acs.est.4c06645
Environ. Sci. Technol. XXXX, XXX, XXX−XXX

(94) Sullivan, K. P.; Werner, A. Z.; Ramirez, K. J.; Ellis, L. D.; Bussard, J. R.; Black, B. A.; Brandner, D. G.; Bratti, F.; Buss, B. L.; Dong, X.; Haugen, S. J.; Ingraham, M. A.; Konev, M. O.; Michener, W. E.; Miscall, J.; Pardo, I.; Woodworth, S. P.; Guss, A. M.; Román-Leshkov, Y.; Stahl, S. S.; Beckham, G. T. Mixed Plastics Waste Valorization through Tandem Chemical Oxidation and Biological Funneling. *Science* **2022**, *378* (6616), 207−211.
(95) Saavedra, J.; Stoll, S.; Slaveykova, V. I. Influence of Nanoplastic Surface Charge on Eco-Corona Formation, Aggregation and Toxicity to Freshwater Zooplankton. *Environ. Pollut.* **2019**, *252*, 715−722.
(96) Wang, L.; Wu, W.-M.; Bolan, N. S.; Tsang, D. C. W.; Li, Y.; Qin, M.; Hou, D. Environmental Fate, Toxicity and Risk Management Strategies of Nanoplastics in the Environment: Current Status and Future Perspectives. *Journal of Hazardous Materials* **2021**, *401*, No. 123415.
(97) Roohi; Zaheer, M. R.; Kuddus, M. PHB (Poly-β-Hydroxybutyrate) and Its Enzymatic Degradation. *Polym. Adv. Technol.* **2018**, *29* (1), 30−40.
(98) Emadian, S. M.; Onay, T. T.; Demirel, B. Biodegradation of Bioplastics in Natural Environments. *Waste Management* **2017**, *59*, 526−536.
(99) Plavec, R.; Hlaváčiková, S.; Omaníková, L.; Feranc, J.; Vanovčanová, Z.; Tomanová, K.; Bočkaj, J.; Kruželák, J.; Medlenová, E.; Gálisová, I.; Danišová, L.; Přikryl, R.; Figalla, S.; Melčová, V.; Alexy, P. Recycling Possibilities of Bioplastics Based on PLA/PHB Blends. *Polym. Test.* **2020**, *92*, No. 106880.
(100) Eronen-Rasimus, E. L.; Näkki, P. P.; Kaartokallio, H. P. Degradation Rates and Bacterial Community Compositions Vary among Commonly Used Bioplastic Materials in a Brackish Marine Environment. *Environ. Sci. Technol.* **2022**, *56* (22), 15760−15769.
(101) Tamaoka, J.; Ha, D.-M.; Komagata, K. Reclassification of Pseudomonas Acidovorans Den Dooren de Jong 1926 and Pseudomonas testosteroni Marcus and Talalay 1956 as Comamonas Acidovorans Comb. Nov. and Comamonas testosteroni Comb. Nov., with an Emended Description of the Genus Comamonas. *International Journal of Systematic and Evolutionary Microbiology* **1987**, *37* (1), 52−59.
(102) Ryan, M. P.; Sevjahova, L.; Gorman, R.; White, S. The Emergence of the Genus Comamonas as Important Opportunistic Pathogens. *Pathogens* **2022**, *11* (9), 1032.
(103) Kenny, S. T.; Runic, J. N.; Kaminsky, W.; Woods, T.; Babu, R. P.; Keely, C. M.; Blau, W.; O'Connor, K. E. Up-Cycling of PET (Polyethylene Terephthalate) to the Biodegradable Plastic PHA (Polyhydroxyalkanoate). *Environ. Sci. Technol.* **2008**, *42* (20), 7696−7701.
(104) Basu, A.; Apte, S. K.; Phale, P. S. Preferential Utilization of Aromatic Compounds over Glucose by Pseudomonas Putida CSV86. *Appl. Environ. Microbiol.* **2006**, *72* (3), 2226−2230.
(105) Karlsson, S.; Hakkarainen, M.; Albertsson, A.-C. Dicarboxylic Acids and Ketoacids Formed in Degradable Polyethylenes by Zip Depolymerization through a Cyclic Transition State. *Macromolecules* **1997**, *30* (25), 7721−7728.
(106) C. Fernandes, A. Reductive Depolymerization as an Efficient Methodology for the Conversion of Plastic Waste into Value-Added Compounds. *Green Chem.* **2021**, *23* (19), 7330−7360.
(107) Johnson, D. R.; Lee, T. K.; Park, J.; Fenner, K.; Helbling, D. E. The Functional and Taxonomic Richness of Wastewater Treatment Plant Microbial Communities Are Associated with Each Other and with Ambient Nitrogen and Carbon Availability. *Environmental Microbiology* **2015**, *17* (12), 4851−4860.

https://doi.org/10.1021/acs.est.4c06645
Environ. Sci. Technol. XXXX, XXX, XXX−XXX